Journal Pre-proof

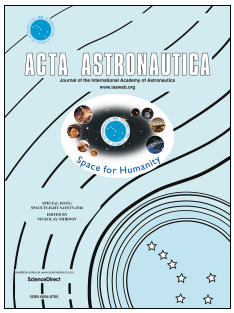

ARTHROSPIRA-C space flight experiment: Validation of biomass and oxygen production bioprocesses using ground model demonstrator system

Jana Fahrion, Cécile Renaud, Ilse Coninx, Wietse Heylen, Felice Mastroleo, Surya Gupta, Guillaume Bayon-Vicente, Ruddy Wattiez, Natalie Leys, Claude-Gilles Dussap

PII: S0094-5765(24)00657-X

DOI: https://doi.org/10.1016/j.actaastro.2024.11.010

Reference: AA 10794

To appear in: *Acta Astronautica*

Received Date: 30 May 2024

Revised Date: 12 October 2024

Accepted Date: 4 November 2024

Please cite this article as: J. Fahrion, C. Renaud, I. Coninx, W. Heylen, F. Mastroleo, S. Gupta, G. Bayon-Vicente, R. Wattiez, N. Leys, C.-G. Dussap, ARTHROSPIRA-C space flight experiment: Validation of biomass and oxygen production bioprocesses using ground model demonstrator system, *Acta Astronautica*, https://doi.org/10.1016/j.actaastro.2024.11.010.

ARTHROSPIRA-C space flight experiment: Validation of biomass and oxygen production bioprocesses using ground model demonstrator system

Jana Fahrion[1,3*], Cécile Renaud[2*], Ilse Coninx[1], Wietse Heylen[1], Felice Mastroleo[1], Surya Gupta[1], Guillaume Bayon-Vicente[2], Ruddy Wattiez[2], Natalie Leys[1**], Claude-Gilles Dussap[3]

[1] Nuclear Medical Applications, Belgian Nuclear Research Center SCK CEN, Mol, Belgium

[2] Proteomics and Microbiology Department, University of Mons, Mons, Belgium

[3] Université Clermont Auvergne, CNRS, Clermont Auvergne INP, Institut Pascal, Clermont-Ferrand, France

* Both authors contributed equally to the study

**corresponding author: natalie.leys@sckcen.be

Abstract

The Micro-Ecological Life Support System Alternative (MELiSSA) project of the European Space Agency develops a biological recycling loop for manned long-term space flight. The air revitalisation and food production are carried out by vascular plants and a photobioreactor containing the cyanobacterium *Limnospira indica*. In the space flight experiment ARTHROSPIRA-C, cultures of *L. indica* are run in a one-week batch mode (45 µmol photons m^{-2} s^{-1}) followed by four semi-continuous cycles of two weeks length. Each cycle has a different, predefined light intensity following an increasing regime (45-55-70-80 µmol photons m^{-2} s^{-1}). In this study, two ground science verification tests (SVT and δ-SVT) were conducted in a laboratory setting to test the reliability and functionality of the hardware- and software of ARTHROSPIRA-C. The SVT explored all four cycles and light intensities and δ-SVT was an additional test where only cycle 1 and 2 were performed. δ-SVT was used to investigate anomalies during SVT. These experiments revealed oxygen production rates between 0.10 ± 0.03 and 0.45 ± 0.01 mmol O_2 L^{-1} h^{-1} and biomass production rates between 0.008 ± 0.000 and 0.021 ± 0.002 g L^{-1} h^{-1} while demonstrating sustained photosynthetic activity at all tested light intensities. In addition, proteomics analysis revealed interesting light intensity-induced effects on multiple pathways, whereas the lipidomic analysis reported no alterations. This study delves into the ground tests conducted during ARTHROSPIRA-C, paving the way for a forthcoming successful flight experiment scheduled aboard the International Space Station in autumn 2024.

Keywords

cyanobacteria, International space station space flight experiment, air revitalisation, photobioreactors, food production, MELiSSA

1. Introduction

As manned space missions become more frequent and longer in duration, the demand for consumables such as water, oxygen, and food for the crew is increasing. To circumvent the high costs and logistic challenges of large cargo, bioregenerative life support systems (BLSS) are needed to recycle

as many organic and inorganic compounds as possible. The cyanobacterium *Limnospira indica* is part of the micro-ecological life support system alternative (MELiSSA) program of the European Space Agency (ESA), and is used for air revitalisation, water recycling, food production and plants biostimulants in this BLSS (Lasseur and Mergeay 2021). The MELiSSA project is inspired by an aquatic ecosystem and includes e.g. thermophilic anoxygenic bacteria, nitrifying bacteria, plants and also cyanobacteria (Lasseur 2008; Hendrickx et al. 2006). *Limnospira indica,* previously called *Arthrospira sp.* or *Spirulina sp.* (Nowicka-Krawczyk, Muhlsteinova, and Hauer 2019) is a filamentous cyanobacterium, capable of producing oxygen through photosynthesis just like other cyanobacteria and plants (Fahrion, Dussap, and Leys 2023). The biomass of *L. indica* is fully edible and high in protein and antioxidants, making it a good candidate as a supplement to other nutrition sources (Wu et al. 2016; Farag et al. 2015). *Limnospira indica* as other photosynthetic bacteria need photons from the visible light spectrum to produce oxygen. Carbon and nitrogen sources such as bicarbonate and nitrate ions are necessary to build up the biomass, therefore ensuring, in parallel to the recycling of CO_2 and O_2 production, an edible biomass production.

The ability to produce oxygen and edible biomass with high production rates and in a cost-efficient manner makes algae and cyanobacteria suitable candidates for BLSS (Niederwieser, Kociolek, and Klaus 2018). BLSS have several advantages over classical cargo-based methods, such as reduced cost and weight. Thus, greater distances can be achieved for human space travel (Fahrion et al. 2021). Physicochemical life support systems, such as the ones tested and used on board the International Space Station (ISS), can also be used to provide space crews with fresh air and water (Junaedi et al. 2011; Takada et al. 2019), but these methods are not sustainable in the long term and are additionally not able to bring fresh food to the table. In the coming long-distance human space flights, most likely a combination of biological and physicochemical methods will be used to ensure that a breakdown of one method does not result in a mission failure (Hauslage et al. 2018). Before BLSS can be used for space crews, the different components, hardware as well as organisms and their interactions need to be tested and understood thoroughly.

A part of this process is the testing of the organisms under space conditions to investigate possible influences of microgravity, space irradiation and upload conditions that include hypergravity and strong vibrations. In the case of the MELiSSA project, the ARTEMiSS project (**Art**hrospira gene **E**xpression study and mathematical **M**odeling on cultures grown in the **I**nternational **S**pace **S**tation) is responsible for the testing of *Limnospira indica* under space conditions (Poughon et al. 2020). To this end, two proof-of-concept experiments are conducted on board ISS: ARTHROSPIRA-B (ArtB) and ARTHROSPIRA-C (ArtC). Both experiments aim to translate the photosynthetic bioprocess of *Limnospira indica* to space using model photobioreactors (PBR). The ArtB experiment was already successfully conducted on board the ISS in December 2017 and showed that a batch configuration at 35 µmol photons m^{-2} s^{-1} and 33°C yields similar biomass and oxygen production rates on ground as in space, when proper mixing is provided to the cyanobacterial cultures (Poughon et al. 2020). Instead of batch and fed-batch cultures studied in ArtB, ArtC concerns a semi-continuous set-up (dilution rate = 0.6 mL h^{-1}) with increasing light intensities (45 - 55 - 70 - 80 µmol photons m^{-2} s^{-1}).

This paper focusses on the new developments of ArtC. This study seeks to address several key questions regarding the continuous cultivation of *Limnospira indica* within the experimental set-up and space hardware. Firstly, we aim to determine whether *L. indica* can be successfully grown for longer durations (9 or 5 weeks, respectively) in a continuous manner. Additionally, we are investigating the expected oxygen production and biomass yield within this system, providing insights into its

efficiency and potential scalability. Another major aspect of the research is the identification of the primary controlling factor of the microbial bioprocess in this set-up (gas or light transfer). Furthermore, we are assessing whether the samples of this set-up are suitable for detailed proteomic and lipidomic analyses and whether the light conditions are influencing *L. indica* as intended, ensuring accurate results for downstream applications. ArtC is currently scheduled to fly to the International Space station (ISS) in 2024. To assure a successful experimental run within the ISS, several experiments have to be performed in a ground laboratory beforehand. The main goal of ArtC is the investigation of the impact of space conditions such as microgravity and increased irradiation on the growth of *Limnospira indica* in semi-continuous cultures. The general metabolic rates are monitored online via biomass and oxygen production rates, while in-depth molecular analyses such as proteomics and lipidomics are done on frozen samples after finalisation of the experiment. In this study, the results of the ground tests of ArtC are presented. During these tests, the feasibility and reliability of the hardware (photobioreactors, PBR) and their ability to sustain a healthy semi-continuous culture are tested thoroughly. The procedure of these on-ground experiments is the same as in space, securing direct comparisons between the obtained data sets. A major difference between the space and ground experiments are the increased irradiation and the microgravity occurring on board the ISS, allowing to see the influence of these parameters on *Limnospira indica* growth during the ArtC experiment. These experiments on Earth as well as in space give insights to the metabolic stability of the culture as well as the adaptation of *Limnospira indica* to different light intensities in a semi-continuous culture mode.

2. Material and methods

2.1 Strain description

The photosynthetic cyanobacterium *Limnospira indica* PCC8005 substrain P3 was used in both experiments described in this study. This strain has straight and long trichomes and was shown to grow healthy and stable at temperatures between 22 and 34 °C and light intensities between 35 and 80 µmol photons m^{-2} s^{-1} (Fahrion, Dussap, and Leys 2023). *L. indica* was grown in Zarrouk medium (starting pH = 9.9) as modified by Cogne et al. (2003). In this study, the carbon source for photosynthesis is dissolved bicarbonate ions in the medium. The sole nitrogen source are nitrate ions. As mentioned, this organism was already used in a previous space flight experiment, ArtB, which flew to the ISS in 2017 and investigated the growth of *L. indica* in a batch regime (Poughon et al. 2020). The inocula used for the SVT and δ-SVT experiments were grown in 250 mL Erlenmeyer flasks in Zarrouk medium. For this, 142.5 mL Zarrouk were mixed aseptically with 7.5 mL of culture (5% inoculation). The inocula were grown at 30°C and 45 µmol photons m^{-2} s^{-1} in a Binder KBWF 720 climate chamber (Analis SA, Belgium) until they reached an OD_{770nm} of 1.18 (SVT) and 1.25 (δ-SVT), respectively.

2.2 Axenicity

All cultures were checked for axenicity in the beginning of the experiments and after each cycle by inoculating 1 mL of culture in 10 mL LB medium and additionally, 1 mL culture in a 9 mL Zarrouk and 1 mL LB mixture, each in 50 mL culture flasks (Greiner BIO-ONE). If there is no visible microbial growth (no turbidity) after 7 days, the cultures were presumed to be axenic. During the 7 days, the flasks resided in Binder incubators at 30°C, 120 rpm and 30 µmol photons m^{-2} s^{-1}. Detected contaminants were plated on LB agar and send for 16S rRNA sequencing (Eurofins).

2.3 Experimental set-up

2.3.1 Experiments

The science verification test (SVT), is an experiment to check the feasibility and reliability of the set-up, hardware, software, and experimental schedule. This test follows the entire procedure of ArtC in a laboratory setting at SCK CEN, Belgium. The first SVT experiment was performed at SCK CEN Microbiology laboratories for 9 weeks active operation (from 03/10/2022 until 05/12/2022) and consisted of a one week batch propagation (45 µmol photons m^{-2} s^{-1}) followed by four semi-continuous cycles of two weeks length with increasing light intensities (45 - 55 - 70 - 80 µmol photons m^{-2} s^{-1}). The second experiment (also performed at SCK CEN) named δ-SVT and was done additionally to SVT to gather more data and to understand and solve problems that occurred during SVT. This run was conducted for 5 weeks (from 15/05/2023 until 19/06/2023), including the one week batch followed by cycle 1 and 2 (45 and 55 µmol photons m^{-2} s^{-1}).

2.3.2. Experiment hardware

The hardware used in the present study was upgraded from the previous space flight experiment ArtB (Poughon et al. 2020) and the design of the operational photobioreactors are based on research from the University of Clermont-Auvergne (Cogne, Cornet, and Gros 2005; Cogne et al. 2001). Similar as ArtB, the ArtC space flight experiment is designed to be executed in the Biolab facility, the ESA multi-user facility for biological experiments on board the ESA Columbus Module, on the International Space Station (ISS). The space and Biolab compatible mini-sized PBRs were manufactured by Redwire Space Europe for ESA. A picture and an operational schematic of the reactors and the set-up can be found in Figure 1. In total, 8 of these reactors are used during the ArtC space flight. Four so-called flight models (FM) will be used onboard the ISS, and four ground models (GMs) will run in parallel on ground. In the experiments presented here, the GMs and their associated feeding and sampling reservoirs were used. The GM reservoirs were emptied and reused during the run. Each reactor has a flat cylindrical culture chamber (CC) of V_{CC}=51.69 ± 1 mL, which contains the active cell culture inside an expandable PFA bag (wall thickness of 127 µm). The culture chamber (CC) is connected to a gas chamber (GC) via a gas-permeable membrane (hydrophobic polytetrafluorethylene (PTFE), 57 ± 1 µm thick, pore size 0.2 µm (Sartorius-Sedim 11807)). This membrane was specifically selected for its high oxygen permeability and has a 26 cm^2 surface, resulting in a liquid volume to surface ratio of 1.96 cm^3/cm^2. The gas chamber (GC) has a volume of V_G=22.37 mL (gas to liquid ratio = 0.43) where the produced oxygen is allowed to accumulate up to a relative overpressure of 150 mbarg, whereby g stands for gauge, or relative pressure versus the static liquid pressure in the CC. To secure optimal gas release and to prevent bubble formation at the liquid side, it was aimed to always maintain the static liquid pressure in the CC higher than the pressure inside the GC (>1.150 bara). This was realised via a peristaltic pump in front of the liquid chamber and a back pressure control valve after the liquid chamber. During δ-SVT, one reactor was additionally run with a venting threshold of 50 mbarg instead of 150 mbarg for 3 days, to test if this lower threshold could be used to ensure that the gas pressure is always lower than the liquid pressure, to improve oxygen release from the liquid to the gas phase, and to reduce the risk of gas bubble formation in the liquid phase. When the threshold is reached, which is monitored by the gas pressure sensor (KULITE XTL-193-190), a pressure valve opens and vents the gas chamber for 30 seconds to secure full pressure release. The gas chamber venting valve is commanded to vent at relative pressure, independent of absolute atmospheric gas pressure between 0.900 and 1.250 bara (bar absolute), at the other side of the venting valve inside the incubator for advanced experiment containers (AECs) on the anti-settling device in Figure 1, or inside the closed AECs connected to Biolab ventilation system in the future. A filter (0.2 µm thickness, 3.1 cm^2 surface, PTFE) is interposed between the GC and the gas sensor and pressure relief valve (0.2 µm thickness, 3.1 cm^2 surface, PTFE). Every time the gas chamber vents, the relative pressure is set to zero. The optical measurement unit (OMU, manufactured and miniaturized by Gademann Instruments) is connected to the CC via tubings and consists of an optical density measurement instrument (Biomass assessment via OD, polycarbonate

172 cuvette, optical path of 5 mm (10mm in ArtB)) and a pulsed amplitude modulated (PAM) fluorometry
173 instrument (Quantum yield measurements, same cuvette, saturation pulse of 6000 µmol photons m^{-2}
174 s^{-1}). The magnetic stirrer bar inside each culture chamber is stirring at a speed of 1000 rpm (in ArtB
175 only 800 rpm were used) and change their direction every 600 seconds (i.e. every 10 min). The stirrer
176 bar is sitting on the surface of the gas permeable membrane, and held in place with a stirrer bar holder
177 cap. During the entire experiment, the culture is illuminated by 36 LEDs (Nichia NESL064AT, full PAR:
178 400 – 700 nm) which can be set to different light flux intensities (45-80 µmol photons m^{-2} s^{-1}). The LEDs
179 are positioned at the cylindrical plane, at the opposite side from the membrane, separated from the
180 CC by a transparent polycarbonate window (26 cm^2 illuminated surface).
181 Each PBR is equipped with a feed reservoir which is filled with 90 mL (double bag reservoir) or 200 mL
182 Zarrouk culture medium (single bag reservoir), a fixed-sample reservoir (filled with 30 mL RNAlater)
183 and an empty sample reservoir (Fig. 1). The feed reservoirs provide fresh Zarrouk culture medium and
184 contain a defined space to collect and store the flow-through of the culture. In case of the single bag
185 reservoirs, the flow through is stored between the outside of the PFA bag which contains the Zarrouk
186 medium and the aluminium shell, and in case of the double bag reservoirs, the flow through is stored
187 in a separate PFA bag next to the Zarrouk bag. Both bags are inside the aluminium shell of the reservoir.
188 The sample reservoirs are used to sample the culture from the CC at the end of each of the four
189 production phases. All sample reservoirs also contain a PFA bag.

190 An anti-settling device (ASD) was used additionally to the internal stirring bar to prevent the formation
191 of sediments and biofilms under Earth gravity conditions. This machine turns the photobioreactors by
192 180° (duration of 5 sec, clockwise and counterclockwise, g vector perpendicular to the gas/liquid
193 interface membrane) every 5 minutes on a horizontal axis (Fig. 1). This device will also be used for the
194 ground control experiments of ArtC. Both experiments were carried out at 33 ± 1°C, by placing the full
195 set-up inside a convective air heated laboratory incubator (Binder incubator at 33°C).

196 All reactors are connected to electronic boxes and finally to a computer with a dedicated software
197 which commands the reactors via a predefined operations timeline and logs the data generated by the
198 reactors. During SVT, the electronic boxes were placed inside the incubators (next to the reactors).
199 This placement was found to induce high variability of the OMU measurements due to the higher
200 temperature and it was therefore decided to place all electronics except the AECs outside of the
201 incubator for the delta-SVT experiment.

202 The software logs the light, temperature (outside CC wall) and stirring as well as the data of the
203 pressure sensor inside the gas chamber minimum once every two seconds. The optical density and
204 fluorescence measurements of the OMU sensor were performed every 9 and 11 hours respectively.

205

206 **2.3.3. Experiment Settings, operations and timeline**

207 The experiments start with the dormancy phase (7-14 days) where the cultures are stored at 4°C in the
208 dark without mixing. In the space flight experiment, this dormancy period is the passive storage period
209 needed to bring the freshly inoculated reactors from the experiment preparation laboratory to the
210 launch site and on-board ISS, and from the docked upload vehicle until the activation in the biolab
211 facility in the Columbus module in ISS. In ArtC as well as during the laboratory tests presented here,
212 the inoculum culture (*Limnospira indica* PCC8005 P3, OD_{770nm} = 1.0-1.3) is introduced in the hardware
213 and stored inside the liquid loop tubings. All tubings of the liquid loop are PharMed biocompatible
214 tubings (BPT) which are less gas-permeable (CO_2, O_2) than silicon tubings and therefore suitable to
215 minimize off-gassing and loss of CO_2 from the media. For this study, the dormancy period was only
216 conducted for SVT, for 11 days. For δ-SVT, this was skipped due to time constraints. To minimize
217 pressure drop due to cooling (which might lead to CO_2 off-gassing from the medium with inoculum in

218 the tubings) after transfer of the AECs to the cold room (4°C, dark), the reactors were left in an open
219 configuration for 24 hours to cool down and closed afterwards. After dormancy, a revival and
220 propagation phase of 7 days in batch mode (45 µmol photons m^{-2} s^{-1}) follows. To start this phase, the
221 inoculum (9 mL) is diluted with 51 mL of fresh Zarrouk medium in the inflatable CC, and the LEDs and
222 the stirrer are activated. During this initial batch, it is aimed to revive the cells after cold storage and
223 to proliferate the small volume inoculum to a larger volume dense culture, with an optical density
224 increasing from OD_{770nm} ~ 0.100 to OD_{770nm} ~ 1.00. This is followed by 4 production phases (called cycles
225 1, 2, 3, 4), with semi-continuous liquid feeding, each with exposure to four different light intensities
226 (45, 55, 70 and 80 µmol photons m^{-2} s^{-1}) and a duration of 2-weeks (340 hours). The pump is activated
227 at a speed of 0.2 mL min^{-1}, for 30 seconds every 10 minutes (*i.e.*, 3 min h^{-1} total on-time at a speed of
228 0.2 mL min^{-1}), resulting in a constant feeding rate during all 4 cycles of 0.6 mL h^{-1}. In between, the pump
229 is turned off. Only right before an OMU measurement (OD and QY, every 9 and 11 hours respectively),
230 a turbidity state is turned on, which mixes the liquid in a closed loop. During this state, the pump is
231 active at a speed of 3 mL min^{-1} for 3 minutes. The volume of the tubings (+ cuvette of OMU) of the
232 liquid circuit is estimated to be $V_{Tubings}$=7.56 mL. Thus, a stable biological process for 3.9 retention times
233 (1 retention time = 51.69 mL/0.6 ml h^{-1} = 86.15 h, total time per cycle = 340 h) is achieved in each cycle.

234 Each culture is sampled every 2 weeks (340 hours), and the goal is to maintain axenicity during the full
235 run of nine (or five) weeks. The RNA later reservoirs are used to fix samples for molecular analysis.
236 These samples are used for proteomics and lipidomics analysis. During ArtC, RNAlater samples will be
237 frozen at -80°C inside their respective sample reservoirs. Additionally, pure, unfixed culture samples
238 will be taken and frozen at -80°C in their respective reservoirs. In the SVT and δ-SVT experiments, only
239 the RNAlater fixed samples were used. These were extracted from their respective reservoirs before
240 freezing to circumvent additional freezing /thawing cycles of the hardware.

241 During the SVT experiment, several problems were identified. To find solutions for these problems, a
242 new test, δ-SVT, was planned and performed. Several changes were implemented for δ-SVT to
243 circumvent the problems detected in SVT. Firstly, the software was adapted to avoid timeline errors.
244 Secondly, the reservoir handling procedure was changed to circumvent development of an
245 underpressure at the waste site. Additionally, manual filling commands were implemented before
246 sampling and reservoir exchange, to additionally maintain the liquid pressure (maximum of 5 mins at
247 3 mL min^{-1}, only in-flow). To improve the precision of the OD values and to counteract high standard
248 deviations, the OMU was newly calibrated. Lastly, the electronics connecting the reactors to the
249 computers were placed outside of the incubators instead of inside.

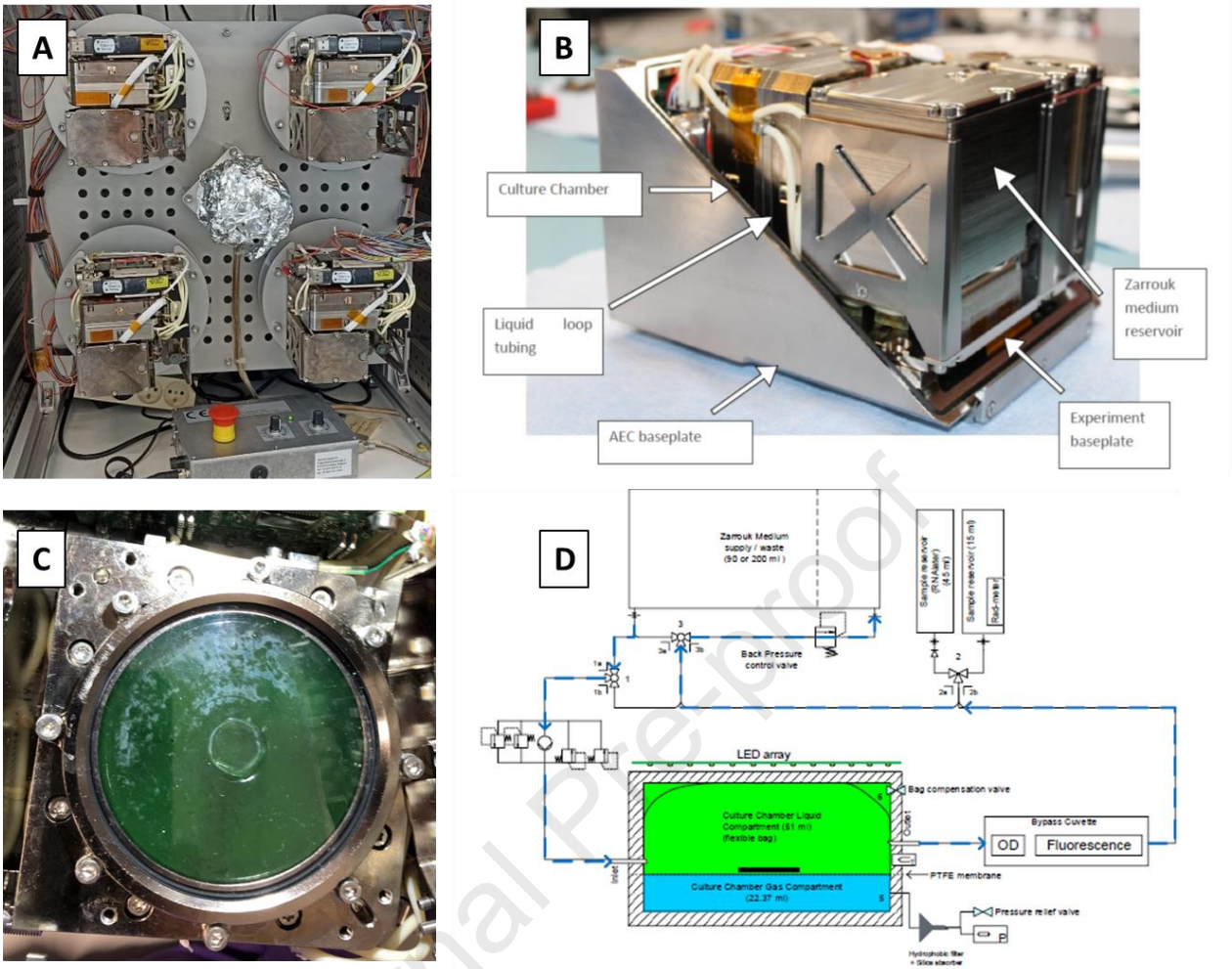

Figure 1. Space compatible miniaturized photobioreactor of the ArtC flight experiment (manufactured by Redwire Space Europe for ESA). A: Picture of the anti-settling device inside incubator, on which 4 AEC are mounted in 'open box' configuration and periodically rotated 180°C to alternate the impact of the gravity vector; B: Picture of the AEC Advanced Experiment Container (containing the photobioreactor) compatible with BIOLAB facility in ISS; C: Top view (from LED array side) into the flat cylindrical culture chamber with flexible bag filled with 51 ± 1 ml green cyanobacterial culture without gas bubbles. D: Schematic of liquid loop allowing feeding to the culture chamber, measurements in a circular by-pass loop over the culture chamber, and sampling from the culture chambers to the reservoirs, all while maintaining liquid pressure; source of B and D: Redwire Space Europe.

2.4 Analysis of collected Online data

2.4.1 Oxygen production

The oxygen production of the cultures was monitored via the gas pressure sensor in the GC. Each venting of the gas pressure relief valve corresponds to the production of 150 mbar O_2 (or 50 mbar for 3 days in 1 reactor during δ-SVT (small test)). The cumulative pressure is the sum of the pressure from all ventings. The oxygen production rate r_{O2} [mmol L^{-1} h^{-1}] was derived by conversion of the cumulative pressure graph (in Pa) to mmol L^{-1} using the ideal gas law applied to the gas chamber (V_G=22.37 mL) and dividing by the total liquid volume (V_L=V_{CC}+$V_{Tubings}$= 59.25 mL). The slope of the resulting curves was obtained by linear regression using EXCEL 2016 data analysis toolpak. r_{O2} was calculated for every reactor for all cycles and the batch phase (Fig. 2), and combined over all reactors per phase (Table 1). For all r_{O2} calculations, the first 90 hours (first residence time 86.15 h + 5%) after start of a new cycle were not included to ensure the data is representative of the steady semi-continuous state. r_{O2} in [g L^{-1} h^{-1}] was obtained by multiplying r_{O2} [mmol L^{-1} h^{-1}] by the molar mass of O_2 (32 [g mol^{-1}]). r_{O2} in [g L^{-1}

273 h^{-1}] was then used to calculate the instantaneous yield of oxygen which was produced per biomass
274 (see section 2.4.3).

275 **2.4.2 Biomass production**

276 The biomass production rate r_X [g L^{-1} h^{-1}] was derived from the OD_{770nm} values which were obtained
277 every 9 hours by the optical measurement unit (OMU). The correlation between OD_{770nm} and biomass
278 [g L^{-1}] was derived beforehand from preliminary batch growth experiments in Erlenmeyer flasks for
279 cultures with OD_{770nm} values between ~0.5 and 1.5 and was shown to be

280 $$\textbf{Biomass concentration X [g L}^{-1}\textbf{] = OD}_{770nm}\textbf{ x 0.6396 + 0.7133} \quad (1)$$

281 Similar to ArtB, three different absorbance measurements were performed. While the OD at 770 nm
282 is used to calculate the biomass concentration (X, g L^{-1}) and production rate (r_X, g L^{-1} h^{-1}) at each OD_{770nm}
283 measuring time point, the OD_{630nm} and OD_{466nm} give qualitative insights into the pigment content of the
284 cultures (630nm: phycocyanin and allophycocyanin; 466nm: chlorophyll a) (Fahrion, Dussap, and Leys
285 2023) and are mainly used to estimate the photon harvesting efficiency of the culture. As a rule of
286 thumb, healthy and axenic *Limnospira indica* PCC8005 P3 cultures show OD_{466nm}/OD_{770nm} and
287 OD_{630nm}/OD_{770nm} ratios between 1.1 and 1.7, with $OD_{466nm}/OD_{770nm} > OD_{630nm}/OD_{770nm}$.

288 To calculate the biomass production rate of the different cycle phases r_X [g L^{-1} h^{-1}], the biomass
289 concentration X [g L^{-1}] was multiplied by the dilution rate D [h^{-1}]. The dilution rate D equals the liquid
290 flow rate (F =0.6 mL h^{-1}) divided by the total liquid volume (V_L = 59.25 mL) so that D = 0.010 h^{-1}. For all
291 OD measurements and biomass production rates, the first residence time (90 h) is not included in the
292 calculation, for the system to adapt to the new conditions, knowing that we aim to investigate steady
293 state conditions. The cycle (semi-continuous phases) data presented in the results section shows the
294 average and standard deviations of all OD and r_X values during one cycle, separately for each reactor
295 (Fig. 2) as well as combined over all reactors in Table 1. During the batch propagation, the dilution rate
296 is zero. Thus, a linear regression of the biomass concentration [g L^{-1}] vs time [h] was performed (EXCEL
297 2016 data analysis toolpak) and the corresponding slopes are shown as mean ± 95%CI (Fig. 2).

298 **2.4.3 Oxygen yield per biomass**

299 Additionally, the oxygen yield per biomass $Y_{O2/X}$ was calculated. This value is the instantaneous yield
300 given by the ratio of r_{O2} (in [g O_2 L^{-1} h^{-1}] instead of [mmol O_2 L^{-1} h^{-}1]) over r_X [g biomass L^{-1} h^{-1}]. The
301 oxygen yield per biomass $Y_{O2/X}$ [g biomass g O_2^{-1}] was calculated per batch or cycle separately for each
302 of the 4 bioreactors separately (Fig. 2), as well as combined over all reactors (Table 1).

303 **2.4.4 Growth model**

304 The biomass production rate r_X, the oxygen production rate r_{O2} and the yield $Y_{O2/X}$ were additionally
305 assessed based on a kinetic and stoichiometric model developed at the University of Clermont-
306 Auvergne (Poughon et al. 2021; Poughon et al. 2020; Cogne, Cornet, and Gros 2005; Cogne et al. 2001).
307 This model is a combination of four parts: A radiative transfer (light) model, which describes the
308 lighting conditions in the CC at different depths, a biological model describing the stoichiometric
309 equations of photosynthetic growth, a liquid/pH model and a gas model describing the evolution of
310 nutrients in the liquid phase and the partial pressure CO_2 and O_2 in the gas phase respectively. When
311 combined, the evolution of the biomass production and oxygen production inside the miniaturized
312 PBRs can be calculated based on the cell density of the inoculum, the added nutrients and photon flux,
313 for batch as well as semi-continuous operation. The model considers the light energy supply limitation,
314 defining a lightened zone and a dark zone into the reaction volume. This leads to the fact that the light
315 flux is the main variable controlling the growth rate when all nutrients are available in excess in the

media (no substrate limitation). Additionally, gas and liquid phases are assumed to be fully mixed. An in-depth overview of the model, its capacities and constraints are found in Poughon et al. (2021).

In order to understand the relation between the biomass production and O_2 production, a simplified stoichiometric equation has been used (Eq. 2) (Fahrion et al. 2021; Poughon et al. 2021; Cogne et al. 2003; Cornet, Dussap, and Gros 1998). It accounts for the conservation of the four elements (C, H, O and N) and the biomass elemental composition is determined considering the biomass dry mass contains 10% carbohydrates. The light energy conversion efficiency, *i.e.*, the photon yield, is considered as an adjusted variable (stoichiometric coefficient *n*) considering that the photon yield strongly depends on the strain and the culture conditions.

$$CO_2 + 0.701\ H_2O + 0.173\ HNO_3 + n\ h\nu\ \rightarrow CH_{1.575}O_{0.459}N_{0.173} +\ 1.381\ O_2 \qquad (2)$$

This relation shows that, when nitrate is used as the sole nitrogen source, 1.381 mol of O_2 are produced per mol of biomass. Using the molar mass, this relation can be converted to grams, resulting in ~1.88 grams O_2 which are produced per gram of biomass. This stoichiometric yield ($Y^*_{O2/X}$) is only dependent on the stochiometric equation and should stay in the same range for different light intensities, if no substrate limitation and no oxygen or light inhibition occurs, which may change then biomass composition and therefore the elements composition.

2.4.5 Quantum yield

The OMU measures the quantum yield (QY) of the culture. This fluorescence measurement is based on a reflective geometry and saturating flash method to measure instantaneous fluorescence (F) and maximum fluorescence (F_m). The QY can be calculated out of these two values by following formula:

$$\textbf{Quantum Yield (QY)} = (F_m - F) / F_m \qquad (3)$$

Where F stands for the instantaneous fluorescence and F_m for maximum fluorescence. The saturating pulse used by the OMU has an intensity of 6000 µmol photons m^{-2} s^{-1} (620 nm, 0.6 seconds). The QY is a qualitative indicator of the well-being of cyanobacterial cultures and should be between 0.3 and 0.6 (Fahrion, Dussap, and Leys 2023; Schuurmans et al. 2015; Allahverdiyeva et al. 2013; Masojídek, Vonshak, and Torzillo 2010; Gao, Yu, and Brown 2007). The higher this value, the higher the photosynthetic capacity and efficiency of the cultures, as it is a measurement of photon harvesting and electron processing efficiency.

2.4.6 Statistics

The calculations and conversions done on the online data were performed using Excel 2016 and the data analysis toolpak. For oxygen production rate, biomass production rate as well as the values of the different optical densities, only the time points 90 h after cycle start were used. Since the quantum yield is not dependent on the biomass density, the first residence time was not excluded for this parameter. The OD values and biomass production rate rX are presented as averages ± standard deviation. If OD or $r_x(1)$ ± SD was shown to be outside OD or r_X (2) ± SD, $r_x(1)$ and $r_x(2)$ are assumed to be significantly different from each other (*). For the O_2 production rate r_{O2}, which was obtained by linear regression, the 95% confidence interval was calculated and used to compare the r_{O2} of the different cycles. If $r_{O2}(1)$ ± 95%CI was shown to be outside $r_{O2}(2)$ ± 95%CI, $r_{O2}(1)$ and $r_{O2}(2)$ are assumed to be significantly different from each other (*). The yield O_2 per gram biomass ($Y_{O2/X}$) is the ratio of the O_2 production rate (rO_2) and the biomass production rate (r_X), therefore error propagation (Eq. 3) was performed to obtain the standard variation of the yields.

$$\Delta Y/Y = \Delta r_{O2}/r_{O2} + \Delta rX/rX \qquad (4)$$

358 Statistical significant differences of the yields were assessed similar to the r_{O2} values, by checking if Y(1)
359 ± 95%CI is overlapping with the Y(2) ± 95%CI value.

360 **2.5 Proteomic analysis**

361 Proteins were extracted from 6 mL of RNA later fixed (defrosted) sample where biomass is harvested
362 in micro-centrifuge column (cartridge) from Preomics iST Sample preparation kit®. Sample preparation
363 (lysis and proteins purification) is performed using Preomics iST Sample preparation kit® following the
364 manufacturer instructions. Pierce™ Peptide Quantification Colorimetric assay was performed to
365 determine peptide quantity in both samples.

366 Protein identification and quantification were performed following a label-free strategy on a UHPLC
367 HRMS platform (Eksigent 2D ultra, AB SCIEX, TripleTOF™ 6600). Peptides (4µg) were separated on a 15
368 cm C18 column (3C18-CL-120, eksigent) using a linear acetonitrile (ACN) gradient [5-35% (v/v), in 75
369 min] in water containing 0.1% formic acid (v/v) at a flow rate of 300 nL min^{-1}. Peptides spectra were
370 acquired in data dependent (DDA) and data independent (DIA, SWATH) acquisition modes. The MS/MS
371 library needed for DIA analysis was built using DDA mode and ProteinPilot™ software
372 (RRID:SCR_018681, version 5.0.1, AB Sciex, United States). The algorithm Paragon (version 5.0.1.0,
373 4874, AB Sciex, United States) was used to search the MaGe Genoscope database restricted to
374 *Limnospira indica* PCC 8005 (Taxon ID = 376219) (Vallenet et al. 2006). For SWATH analysis, 100
375 incremental steps were defined as windows variable m/z values over a 400/1250 m/z mass range. The
376 MS/MS working time for each window was 7 ms, leading to a duty cycle of 2.65 s per cycle. The ion
377 chromatogram of the top six fragments of each peptide was extracted, and their area under the curve
378 was integrated. Skyline® software (version 22.2.0.527 (841287d47)) (MacLean et al. 2010) was used
379 for the SWATH processing of all proteins identified considering an FDR below 1%. Only proteins
380 quantified with 2 or more peptides were considered in the following analysis. Only fold change, the
381 ratio of the expression of a protein between two cycles, higher than 1.5 or lower than 0.66 and having
382 a *p-value* lower than 0.05 were further considered.

383 **2.6 Lipidomic analysis**

384 Lipids analysis was performed using 6 mL of RNA later fixed (defrosted) Ground Model sample filtrated
385 on 0.2 µm membrane (Sartorius®, cellulose nitrate filters) to harvest the biomass on the filter. After
386 lyophilisation using a freeze dryer (FINN-AQUA®, LYOVAC GT 2E) of the filter, the biomass was
387 resuspended in 1mL H_2O ULC-MS grade. The extraction was carried out with a Methanol-
388 Dichloromethane (respectively 2 mL and 900 µL) mixture by vortexing. 1 mL H_2O ULC-MS grade was
389 added, as well as 900 µL Dichloromethane, vortexed and centrifuged 10 min at 1200 rpm. The organic
390 phase was conserved in an Eppendorf tube. Next, 2 mL Dichloromethane was added again, and
391 centrifugation was performed a second time. The organic phase was harvested once again. Then, the
392 solvent was evaporated using a speedvac (Christ®, RVC 2-18 CDplus) for 2 hours at 45°C. Vials were
393 prepared by resuspending samples in injection solvent (Acetonitrile 60%, Formic acid 0,1%) (dilution
394 100X). Lipid extracts were stored at − 20 °C prior to analysis.

395 Liquid chromatography was performed using a Sciex Exion LC HPLC. All samples were separated on an
396 Phenommenex® column (Synergi™ 4 µm Fusion-RP 80 Å, 50 x 2 mm). The solvent system consisted of
397 two mobile phases as follows: mobile phase A (Acetonitrile 60%, formic acid 0.1%) and mobile phase
398 B (Isopropanol 90%, Acetonitrile 9.8%, formic acid 0.1%). The column operated at a flow rate of 0.6 mL
399 min^{-1} and at 40 °C. The gradient elution program was as follows: 0.01–2 min, 85-70% A; 2–2.5 min, 70-
400 52% A; 2.5–11 min, 52–18% A; 11-12min 18-1% A.

401 Mass spectrometry was performed on a high-resolution mass spectrometer (SCIEX ZenoTof 7600)
402 acquiring data in full scan ion mode and tandem MS/MS using an electrospray ionisation (ESI) source.
403 Fragmentation was performed using collision-induce dissociation (CID). MS was operated using a
404 positive mode (collision energy voltage -10 V, electrospray voltage -4500 V, declustering potential -80
405 V) and negative mode (collision energy voltage 10 V, electrospray voltage 5500 V, declustering

potential 50 V) modes, with a source temperature of 500 °C. Positive and negative modes are used to detect all positively and negatively charged lipids. The following MS/MS used the Zeno configuration and a collision energy of -12 V and declustering of -80 V in negative mode and 12 V in positive mode and declustering of 50 V.

The software MSDial (Tsugawa et al. 2015) (version 4.70, Lipid Maps®, https://www.lipidmaps.org/) was used for lipid identification. The Fiehn O (*VS*68) database (Shitut et al. 2022; Tsugawa et al. 2020) was used to align the data and identify the different lipids, were negative ions were identified as $[M - H]^-$ and positive ions were identified as $[M + H]^+$ and $[M + NH4]^+$ ions. The statistical significance of the diversity was performed by ANOVA (p-value < 0.05).

2.7 Data availability

All computed data for proteomic and lipidomic analysis, as well as raw data, were uploaded to the MassIVE repository (data set identifier MSV000094881) and are freely accessible (https://massive.ucsd.edu/ProteoSAFe/dataset.jsp?task=1b53faa1eebf41cb829009422078cffd).

3. Results

3.1 Bioprocess efficiency

The SVT experiment was started with the same inoculum for all 4 PBRs. The inoculum culture had an OD_{770nm} of 1.18, OD_{630nm} of 1.73 and OD_{468nm} of 1.78 and pH of 10.48. These parameters were assessed on the day of start of the dormancy period, which lasted for 11 days (4°C, dark, no mixing). The δ-SVT experiment was conducted with a similar inoculum culture compared to SVT. The inoculum used had an OD_{770nm} of 1.25, OD_{630nm} of 1.80 and OD_{468nm} of 1.90. The starting pH was 10.58. In the δ-SVT experiment, no cold storage was performed prior to the batch propagation phase. Also, the batch was followed by two cycles of 2 weeks length, with a light intensity of 45 and 55 µmol photons m^{-2} s^{-1}, respectively (similar to cycle 1 and 2 of SVT). The data discussed in the following section were obtained from the batch phase and the 4 semi-continuous cycles, and batch phase and 2 semi-continuous cycles in case of δ-SVT. During the run of the SVT experiment, at some time points problems with the light settings occurred, r_{O2} values during these short periods are not included in the calculations. An overview of these events can be found in the Supplementary Data 1 (Figure S1-S8).

The oxygen production rate r_{O2}, oxygen yield per unit of DW biomass ($Y_{O2/X}$) and biomass production rate (r_X) are shown in Figure 2. The first residence time of the culture in a new light intensity (90 h) is not included in the calculations to exclude possible effects of the transition phase. In SVT, r_{O2} and r_X are lower in the batch phase and stay mostly stable between the different cycles, and in δ-SVT, r_X is also lower in the batch phase but the r_{O2} values are more similar in all phases. Generally, many significant differences between the reactors were detected. Thus, the data sets of the different reactors should not only be viewed combined as averages over all reactors, but also separated to reach an as representative as possible view of the results.

Figure 2 shows that the biomass production rate of GM02 is much lower than the other reactors. This can also be seen in the OD_{770nm} values (Fig. 3). The lower r_X values also result in much higher yield values for this reactor, because $Y_{O2/X}$ is the ratio of oxygen produced per gram biomass. The low OD_{770nm} online values of GM02 in SVT should not be interpreted on a biological level, because the analysis of the flow through of the SVT cultures showed that the offline measured OD_{770nm} values of GM02 are similar to the other cultures (Supplementary Data 1 Tables S1-S4). For example, the flow through (offline measurements) of GM02 after cycle 1 of SVT showed an OD_{770nm} of 0.46. For comparison, GM01 had an OD_{770nm} of 0.66, GM03 had an OD_{770nm} of 0.33 and GM04 had an OD_{770nm} of 0.54. This indicates

that a technical problem caused the low online OD_{770nm} values of GM02. Fortunately, this issue could be resolved by repeating the calibration of the OMUs before the start of δ-SVT (Fig. 2F and 3D).

In SVT, GM02 was found to be non-axenic at the start and endpoint of the experiment and in δ-SVT, GM01 was found to be non-axenic from start until the end, while GM04 showed a contamination in one of the sampling reservoirs. The contaminating microorganism was grown on LB agar plates and send for 16S rRNA sequencing. The sequences of all three contaminants had a 99% sequence identity to a sequence of a *Alkalihalobacillus lindianensis* strain, that was reported to be alkaliphilic and halotolerant, and to grow optimally at 37°C and a pH of 9.0 (Dou et al. 2016).

At the end of cycle 3 of SVT, a software error induced wrong light and pump settings of all 4 reactors. In this period, which lasted for 24 hours, the pump had a speed of ~2.2 ml h^{-1}, which caused a strong dilution of the cultures. This dilution was also verified by weighing of the flow through. Approximately 39 mL of additional flow through were found. In this error phase, the light was set to very low light intensity of 25 µmol m^{-2} s^{-1}.

In δ-SVT, GM02 had to be restarted due to technical problems and thus, only the batch propagation phase followed by cycle 2 was conducted. Figure 3 shows that during SVT, the optical density of the cultures decreased with increasing light flux for all measured wavelengths. The standard deviation is high for the OD values, even though all biological impossible data were removed from the data set (OD < 0 and OD > 3.0). In δ-SVT, the OD values stay similar between the two different light conditions. In δ-SVT, GM04 did not yield in usable OD_{630nm} and OD_{466nm} values (all below 0, technical problem). Generally, the OD_{630nm} and OD_{466nm} values are often lower than expected in comparison to the OD_{770nm} (except for GM02 in SVT), meaning that the OD_{630nm}/OD_{770nm} and OD_{466nm}/OD_{770nm} ratios are lower than expected. An expected range for both ratios is 1.1-1.7, with $OD_{466nm}/OD_{770nm} > OD_{630nm}/OD_{770nm}$, but the SVT results showed ratios between 0.89 and 1.50 (without GM02, which showed ratios above 10), and in δ-SVT, ratios between 0.74 and 1.74 were found. Also, the expectation that $OD_{466nm}/OD_{770nm} > OD_{630nm}/OD_{770nm}$ could not be verified in all reactors and phases. For example, Figure 3F shows that in δ-SVT, the OD_{466nm} of GM02 was lower than the OD_{630nm}.

The QY of the SVT cultures decreased over time (Fig. 4), indicating a slight decline in photosynthetic activity. The QY in all cycles is however still in the expected range for *L. indica* (0.3-0.5, (Fahrion, Dussap, and Leys 2023)). The culture of GM01 generally showed lower QY values in SVT and δ-SVT. In δ-SVT, the QY did not decline between the 2 different tested phases.

OD, r_{O2}, $Y_{O2/X}$ and r_X were all expected to slightly increase with the increasing light flux, but the data showed a decrease of OD and r_X in SVT and a stagnation in r_{O2} and $Y_{O2/X}$. In δ-SVT, all parameters stayed stable for the 2 tested light intensities. Nevertheless, the data clearly shows an active photosynthetic bioprocess in all phases. Visible inspection of the culture chambers at the end of SVT, showed the CCs of GM01 and GM03 had a deflation and the CC of GM04 contained several gas bubbles (Figure 5). The culture chambers of the 4 GMs showed no visible deflation after δ-SVT, but GM01 showed a few bubbles in the CC, and GM04 showed less biomass than the others (Figure 5).

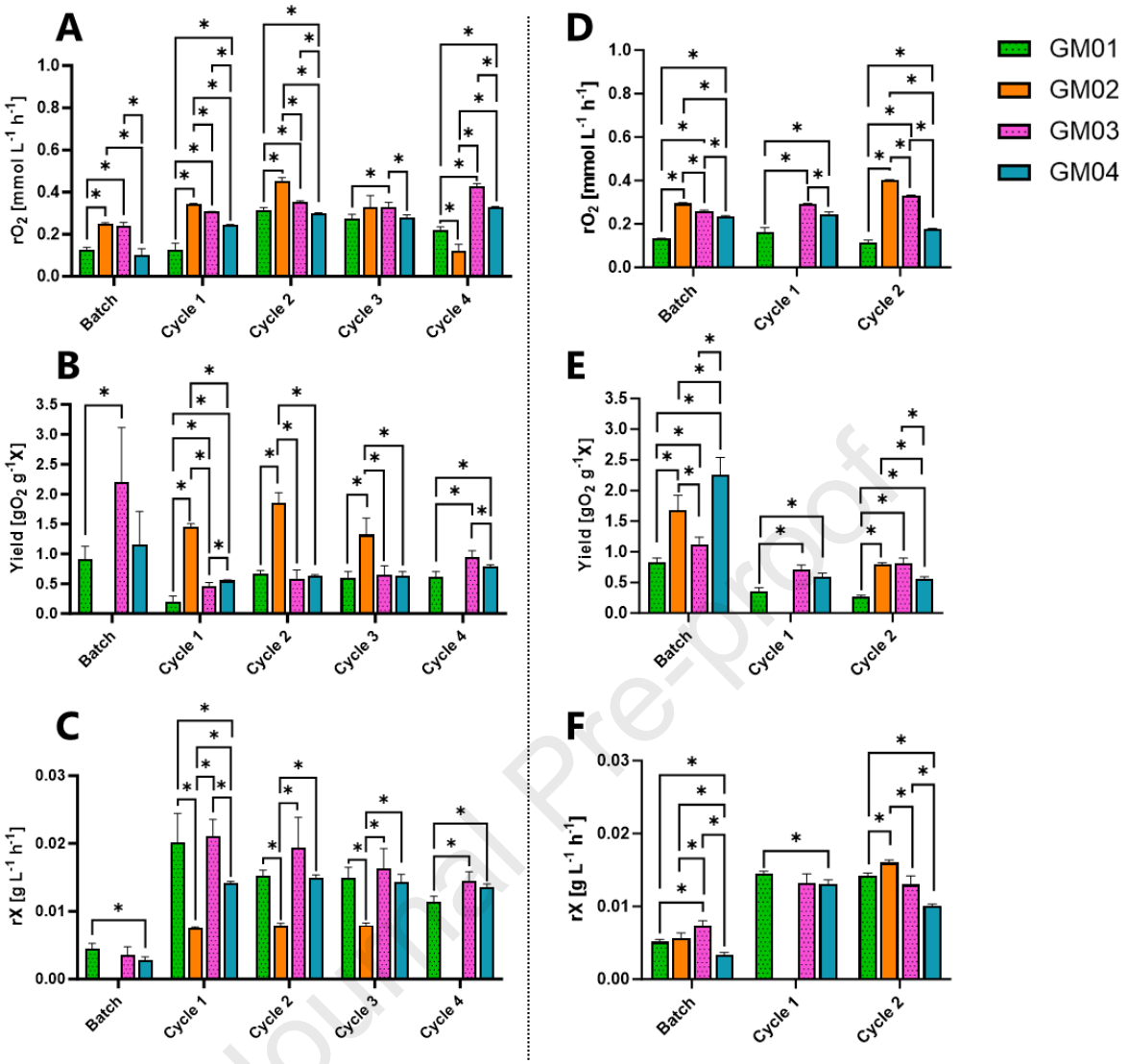

Figure 2. Oxygen production rate r_{O2} (A, D), yield $Y_{O2/X}$ (B, E) and biomass production rate r_X (C, F) per reactor in SVT (A,B,C) and δ-SVT (D,E,F). The first residency time (90 h) was not considered. Statistical analysis was performed using comparison of ±95%CI intervals (r_{O2} and $Y_{O2/X}$) and comparison of ±SD intervals (rX).

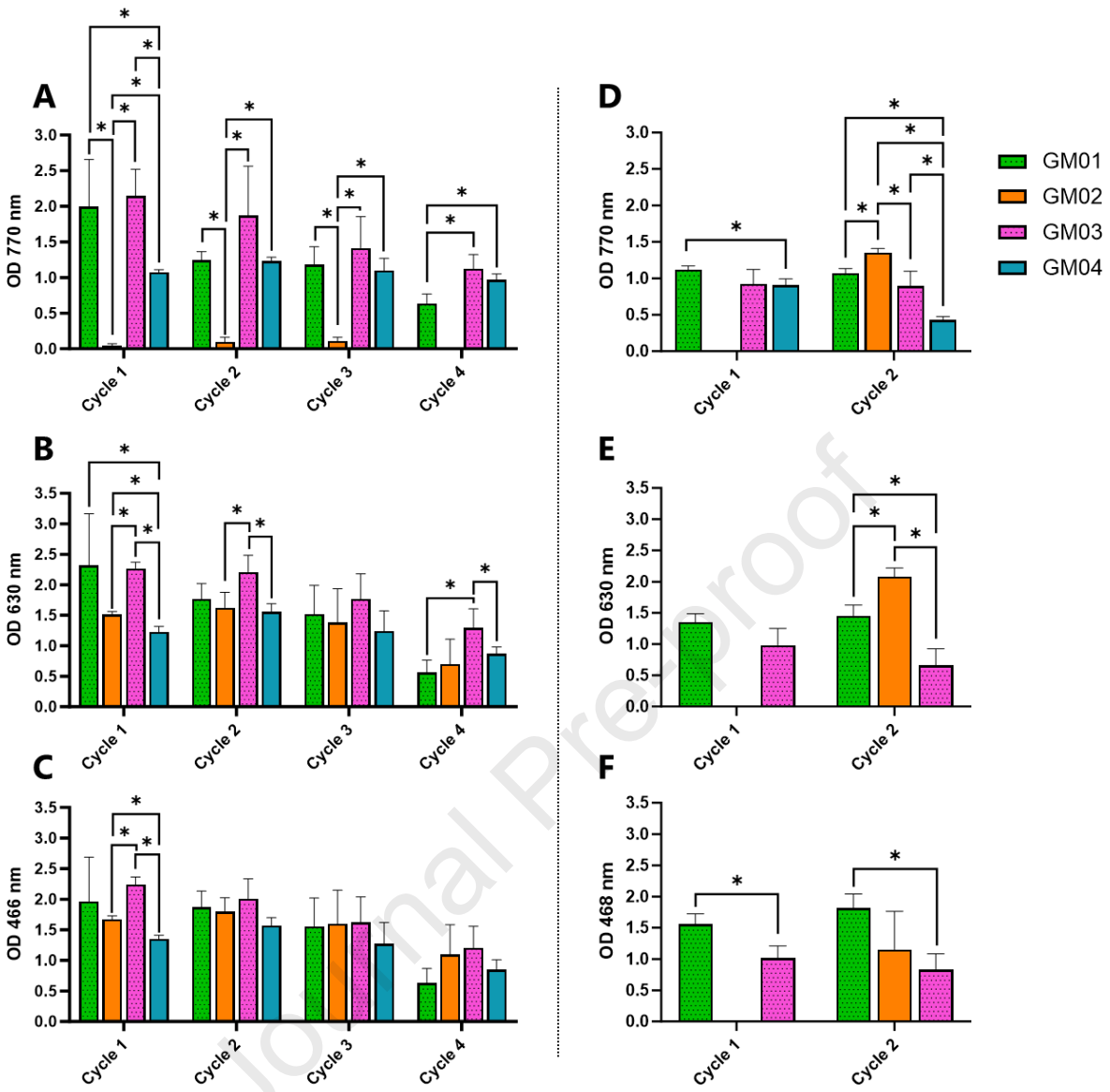

Figure 3. Absorbance of the L. indica cultures at 770 nm (A,D), 630 nm (B,E) and 466 nm (C,F) during the SVT (A,B,C) and δ-SVT experiment (D,E,F). The values are shown as mean ± SD. Only biologically relevant values were used (OD > 0 and OD < 3.0) and the first residency time was removed (90 h). Statistical significance was tested using comparison of ±SD intervals.

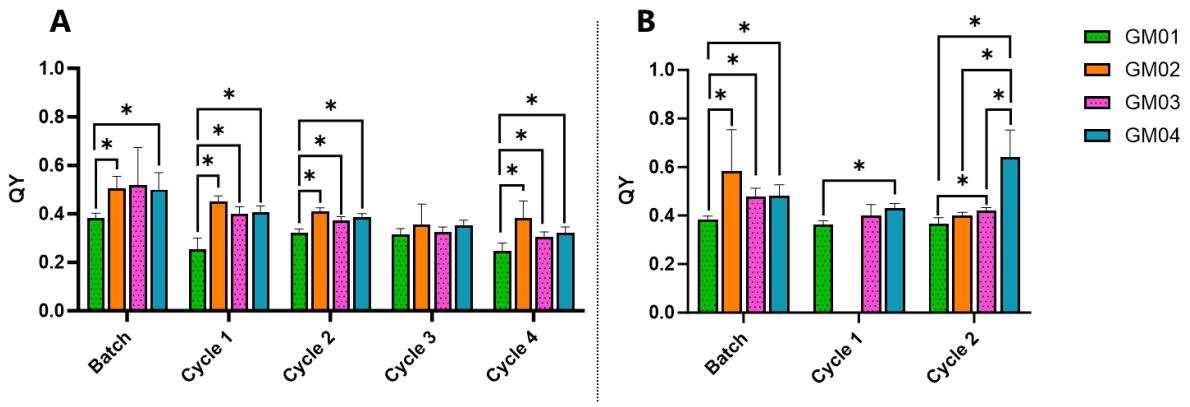

Figure 4. Quantum yield QY during SVT (A) and δ-SVT (B). Biologically impossible data (QY > 1 and QY < 0) were removed. Statistical significance was tested using comparison of ± SD intervals.

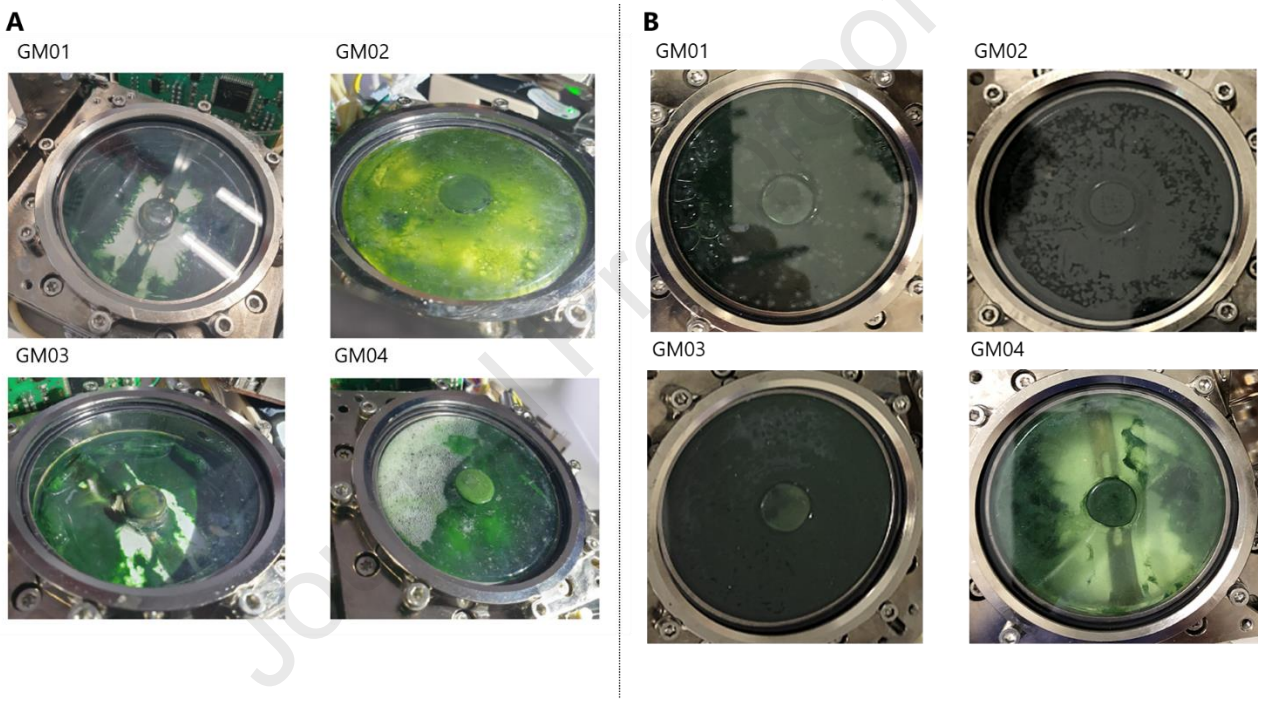

Figure 5. Culture chambers of the 4 ground models (GM) at the end of the SVT (A) and δ-SVT (B) experiments.

3.1.3 Comparison of online data

Table 1 gives an overview of the obtained online data during SVT and δ-SVT. The data presented are grouped per cycle, meaning the different reactors were treated as biological replicates, which leads to a higher variability of the data (see Figure 2, 3 and 4 for comparison). Nevertheless, it helps to quickly compare between the experiments.

The oxygen production rate r_{O2} was significantly lower in δ-SVT than in SVT in cycle 1 and additionally, a non-significantly lower biomass production rate r_X was found in δ-SVT compared to SVT in both cycles. The yield $Y_{O2/X}$ was similar in SVT and δ-SVT, but it can be seen that the yield is higher in cycle 2 when compared to cycle 1. In SVT, r_{O2} and $Y_{O2/X}$ show an increase between cycle 1 and cycle 2 and 3 and 4, but a decrease between cycle 2 and 3. Comparing the obtained values with the theoretical values calculated by the model developed by UCA (Tab. 1, right) (Poughon et al. 2021), it becomes clear

that r_X lies in the expected range while r_{O2} and $Y_{O2/X}$ were found to be lower than expected. Table 1 also shows that all OD values were higher in SVT than in δ-SVT, in both cycles, but none of these data points were found to be significantly different (high variability). The QY was a bit higher in δ-SVT during the second cycle (0.43 ± 0.10 in δ-SVT *vs* 0.37 ± 0.04 in SVT), but this difference was also found to be non-significant. All QY values are in the healthy range for *L. indica* (0.3-0.5).

Table 1. Comparison of the data from SVT, δ-SVT and predicted values from the model developed at UCA (Poughon et al. 2021). Values are shown as mean ± SD (OD, QY, r_X) and mean ± 95%CI (r_{O2} and $Y_{O2/X}$) during one cycle, treating the four different reactors as biological replicates. Statistical significance was tested using comparison of ± SD intervals (OD, QY, r_X) and 95%CI interval comparisons (r_{O2} and $Y_{O2/X}$). Asterix indicate significant difference between SVT and δ-SVT (per light intensity). [1] *QY range was established in our previous study using batch experiments (Fahrion, Dussap, and Leys 2023).*

	SVT (45 µmol photons m^{-2} s^{-1})	δ-SVT (45 µmol photons m^{-2} s^{-1})	EST (45 µmol photons m^{-2} s^{-1})	SVT (55 µmol photons m^{-2} s^{-1})	δ-SVT (55 µmol photons m^{-2} s^{-1})	EST (55 µmol photons m^{-2} s^{-1})	SVT (70 µmol photons m^{-2} s^{-1})	SVT (80 µmol photons m^{-2} s^{-1})	Predicted values
rO_2 [mmol L^{-1} h^{-1}]	0.31 ± 0.02$^{a,\chi,\omega}$	0.26 ± 0.02$^{b,\tau}$	0.29 ± 0.01$^{ab,\rho}$	0.36 ± 0.02$^{a,\psi}$	0.34 ± 0.03$^{a,\upsilon}$	0.26 ± 0.03$^{b,\rho}$	0.28 ± 0.02$^{\chi}$	0.34 ± 0.03$^{\psi,\omega}$	0.58-0.96
Y [$gO_2g^{-1}X$]	0.62 ± 0.26$^{a,\chi}$	0.61 ± 0.09$^{a,\tau}$	0.60 ± 0.07$^{a,\rho}$	0.84 ± 0.29$^{a,\chi}$	0.81 ± 0.21$^{a,\tau}$	0.71 ± 0.15$^{a,\rho}$	0.65 ± 0.19$^{\chi}$	0.83 ± 0.18$^{\chi}$	1.80-1.88
rX [g L^{-1} h^{-1}]	0.016 ± 0.006$^{a,\chi}$	0.014 ± 0.001$^{a,\tau}$	0.016 ± 0.001$^{a,\rho}$	0.014 ± 0.004$^{a,\chi}$	0.013 ± 0.002$^{a,\tau}$	0.012 ± 0.001$^{a,\varsigma}$	0.014 ± 0.003$^{\chi}$	0.013 ± 0.002$^{\chi}$	0.010-0.016
OD_{770nm}	1.35 ± 0.90$^{a,\chi}$	0.98 ± 0.16$^{a,\tau}$	1.29 ± 0.16$^{a,\rho}$	1.03 ± 0.61$^{a,\chi}$	0.94 ± 0.36$^{a,\tau}$	0.70 ± 0.16$^{a,\varsigma}$	1.94 ± 0.47$^{\chi}$	0.91 ± 0.21$^{\chi}$	-
OD_{630nm}	1.83 ± 0.64$^{ab,\chi\psi}$	1.19 ± 0.25$^{a,\tau}$	1.91 ± 0.33$^{b,\rho}$	1.71 ± 0.29$^{a,\chi}$	1.44 ± 0.63$^{ab,\tau}$	0.91 ± 0.31$^{b,\varsigma}$	1.46 ± 0.49$^{\chi\psi}$	0.86 ± 0.39$^{\psi}$	-
OD_{466nm}	1.81 ± 0.50$^{ab,\chi\psi}$	1.31 ± 0.31$^{a,\tau}$	2.10 ± 0.39$^{b,\rho}$	1.77 ± 0.27$^{a,\chi}$	1.69 ± 0.66$^{ab,\tau}$	1.11 ± 0.33$^{b,\varsigma}$	1.52 ± 0.46$^{\chi\psi}$	0.96 ± 0.40$^{\psi}$	-
QY	0.38 ± 0.08$^{a,\chi}$	0.40 ± 0.03$^{a,\tau}$	0.38 ± 0.02$^{a,\rho}$	0.37 ± 0.04$^{a,\chi}$	0.43 ± 0.10$^{a,\tau}$	0.34 ± 0.03$^{a,\rho}$	0.34 ± 0.04$^{\chi}$	0.31 ± 0.06$^{\chi}$	0.30-0.50[1]
α-value	0.10 ± 0.01$^{ac,\chi}$	0.13 ± 0.01$^{b,\tau}$	0.11 ± 0.00$^{c,\rho}$	0.12 ± 0.00$^{a,\chi}$	0.13 ± 0.01$^{a,\tau}$	0.10 ± 0.00$^{b,\varsigma}$	0.11 ± 0.01$^{\chi}$	0.11 0.01$^{\chi}$	-

3.2 SVT Proteomics analysis

The primary objective of the proteomics analysis was to map the overall proteomic profile of the cultures when grown in the specific bioreactor set-up, and to investigate the response of *L. indica* PCC 8005 P3 to different light flux intensities in the photobioreactors. All cultures have been started from the same inoculum (OD_{770nm} = 1.18) and were harvested at the end of the respective cycles. The proteomics analysis was only performed on the SVT experiment. The samples of GM02 which was not axenic were not considered in this analysis, as it had a significant different protein profile (Supplementary data 1, Figure S10). The analysis was focused on the comparison of cycle 1 *vs* cycle 3

532 and 4 (cycle 2 was not included for statistical reasons due to the insufficient sample size, the volcano
533 plot of cycle 2 vs cycle 1 can be found in Supplementary Data 1, Figure S9.

534 According to the UniProt database, 5,722 genes coding for a protein have been identified in *L. indica*
535 PCC 8005. Out of which total 1473 proteins (26% of known proteins) were identified with a FDR below
536 1% amongst all conditions. For quantification analysis, proteins with a fold change lower than 0.66 or
537 higher than 1.5 and with *p-value* ≤ 0.05 were considered as significantly differentially expressed
538 proteins. These 1473 identified proteins were further used to detect differentially expressed proteins
539 in Cycle3 and Cycle4 with respect to Cycle1. For the first comparison between cycle 3 (70 µmol photons
540 m^{-2} s^{-1}) and cycle 1 (45 µmol photons m^{-2} s^{-1}) 1,028 proteins were identified and further used for
541 quantification analysis, revealing a total of 16 significantly differentially expressed proteins (0.02%).
542 Amongst the 16 proteins, 13 showed a higher expression and 3 presented a lower expression in cycle
543 3. The comparison between cycle 4 (80 µmol photons m^{-2} s^{-1}) and cycle 1, 1,013 proteins were
544 identified and further used for quantification, revealing a total of 43 significantly differentially
545 expressed proteins (0.04%). Amongst them, 25 showed a higher expression and 18 presented a lower
546 expression in cycle 4. As presented in the Venn Diagram in Figure 6, 4 proteins presented a significant
547 higher expression (Figure 6A) shared by cycle 3 *vs* cycle 1 and cycle 4 *vs* cycle 1, while 6 presented a
548 significant lower expression (Figure 6B) shared by cycle 3 *vs* cycle 1 and cycle 4 *vs* cycle 1. In addition,
549 volcano plots presented in Figure 6C and 6D, showed that the biggest difference at the proteomic level
550 is observed between the cultures with the biggest variation in light intensity. Indeed, considering the
551 comparison of cycle 3 and cycle 4 against the control (cycle 1), the number of proteins statistically
552 significantly impacted from cycle 3 and cycle 4 were respectively 3 times higher. Data for cycle 2 are
553 available in the repository MSV000094881.

554

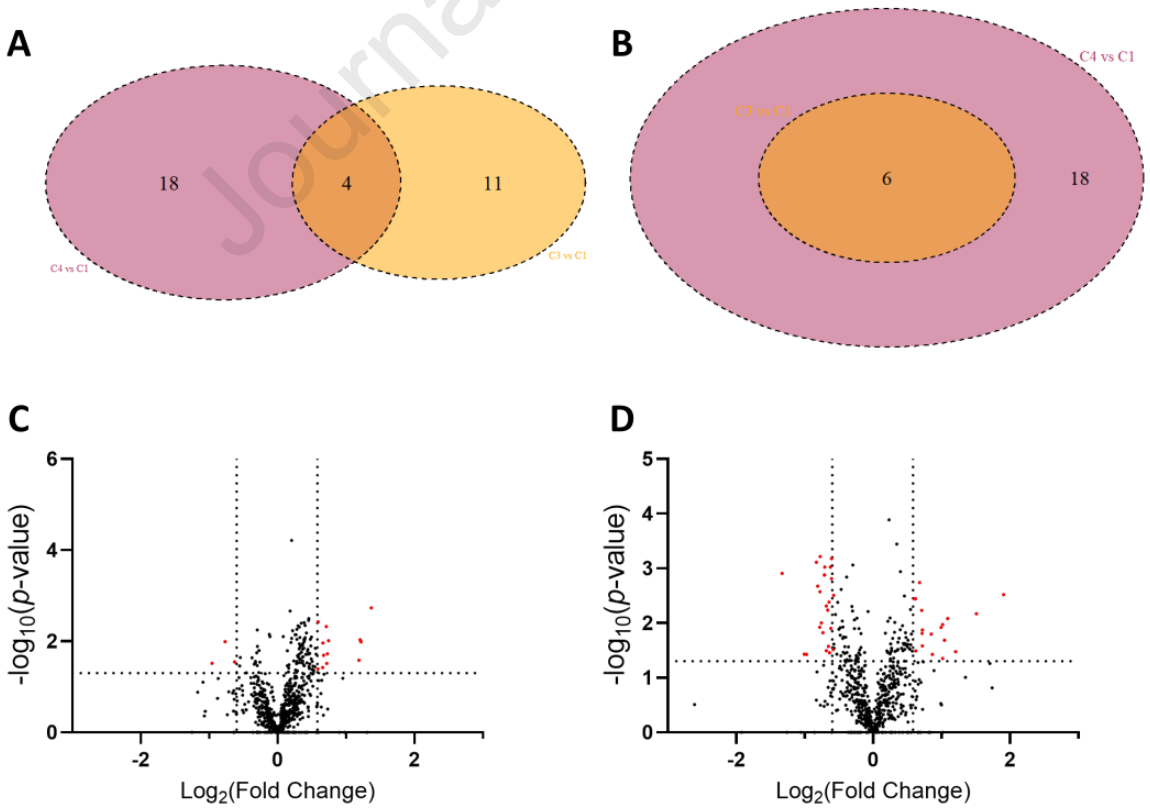

555

556 *Figure 6. Differentially expressed proteins. (A) and (B) Venn Diagrams presenting the number of shared proteins within cycle*
557 *3 vs cycle 1 and cycle 4 vs cycle 1; (A) proteins presenting a higher fold change; (B) proteins presenting a lower expression. (C)*
558 *and (D) Volcano plots of the proteins quantified with significantly differential abundance between L. indica PCC8005 P3*
559 *cultures grown in different cycles associated with different light flux intensity. -log10 (p-value) is plotted against log2 (Fold*
560 *Change). The non-axial vertical lines indicate the ± 1.5-Fold Change (prior to logarithmic transformation) while the non-axial*
561 *horizontal line indicates the p-value ≤ 0.05 (prior to logarithmic transformation) corresponding to the significance threshold*
562 *used in this analysis. All cycles were compared to cycle 1 (45 µmol photons m-2 s-1). (C) Cycle 3 (70 µmol photons m-2 s-1)*
563 *versus cycle 1; (D) Cycle 4 (80 µmol photons m-2 s-1) versus cycle 1.*

564 To clarify the impact of differential light flux intensity on *L. indica* within the SVT experiment at a
565 proteomic level, a more detailed analysis was done on proteins presenting a differential expression
566 between the control cycle (cycle 1) and cycles 3 and 4. The proteins discussed hereafter, from cycle 3
567 and 4, identified as being part of nitrogen metabolism and photosynthesis are presented in Table 2
568 (table including all impacted proteins is in the repository MSV000094881). The focus was on proteins
569 that are statistically (*p*-value ≤ 0.05) and significantly (Fold change ≤ 0.66 or ≥ 1.5) impacted. Also,
570 proteins that displayed a tendency to be impacted, with a fold change close to the threshold (1.5 >
571 Fold change ≥ 1.3 or 0.8 ≥ Fold change > 0.66) and a *p-value* ≤ 0.05, were included.

572 *Table 2. Differential expression of proteins from nitrogen metabolism and photosynthesis in L. indica PCC 8005 P3 cultivated*
573 *under different light flux intensity during SVT experiment. All cycles were compared to cycle 1 (45 µmol photons m^{-2} s^{-1}). (A)*
574 *Cycle 3 (70 µmol photons m^{-2} s^{-1}) versus cycle 1; (B) Cycle 4 (80 µmol photons m^{-2} s^{-1}) versus cycle 1. The fold change is the*
575 *ratio of the abundance of a protein in cycle 3 (A) or cycle 4 (B) to the abundance in the control cycle (cycle 1). (Red = fold*
576 *change ≤ 0.66; Orange = fold change ≤ 0.8; Dark Green = fold change ≥ 1.5; Light Green = fold change ≥ 1.3. ND = Not detected,*
577 *NS = not statistically significant).*

Accession Number		Proteins codes	Protein Description	Number of identified peptides	(A) Cycle 3 *vs* Cycle 1		(B) Cycle 4 *vs* Cycle 1	
MaGe Genoscope	UniProt				Fold Change	p-value	Fold Change	p-value
Photosynthesis								
ARTHROv5_11557|ID:18394976|cpcD|	A0A9P1KD43	CpcD	Phycobilisome 8.9 kDa linker polypeptide, phycocyanin-associated, rod (Rod-capping linker protein)	5	**0,587**	0,010	**0,610**	0,001
ARTHROv5_40726|ID:18397420|cpcG|	A0A9P1NZW8	CpcG	phycobilisome rod-core linker protein	12	**0,646**	0,028	**0,585**	0,001
ARTHROv5_10637|ID:18394056|apcA|	A0A9P1KBV0	ApcA	Allophycocyanin alpha subunit	9	ND	ND	**0,622**	0,032
ARTHROv5_61214|ID:18399719|apcE|	A0A9P1KLD0	ApcE	Phycobiliprotein	36	0,828	NS	**0,670**	0,003
ARTHROv5_12132|ID:18395551|apcF|	A0A9P1NY87	ApcF	allophycocyanin beta-18 subunit	6	0,863	NS	**0,640**	0,004
ARTHROv5_11993|ID:18395412|psbD1|	A0A9P1KDV6	PsbD1	Photosystem II D2 protein (PSII D2 protein) (Photosystem Q(A) protein)	3	0,815	NS	**0,591**	0,010
ARTHROv5_10482|ID:18393901|	A0A9P1KAP7	PsbQ	conserved protein (secreted) - Photosystem II protein	5	0,830	NS	**0,631**	0,006
ARTHROv5_60553|ID:18399058|psbE|	A0A9P1P2R9	PsbE	Cytochrome b559 subunit alpha (PSII reaction center subunit V)	2	0,806	NS	**0,600**	0,015
ARTHROv5_10235|ID:18393654|psaC|	A0A9P1KAU3	PsaC	Photosystem I iron-sulfur center (Photosystem I subunit VII) (9 kDa polypeptide) (PSI-C)	2	0,856	NS	**0,583**	0,003
ARTHROv5_30080|ID:18395909|psaD|	A0A9P1NYA0	PsaD	Photosystem I reaction center subunit II (Photosystem I 16 kDa polypeptide) (PSI-D)	6	0,685	0,023	**0,562**	0,001
ARTHROv5_30657|ID:18396486|psaF|	A0A9P1NZN0	PsaF	Photosystem I reaction center subunit III precursor (PSI-F)	5	0,790	NS	**0,611**	0,001
ARTHROv5_40121|ID:18396815|bchM|	A0A9P1KFC3	BchM	Mg-protoporphyrin IX methyl transferase (bacteriochlorophyll biosynthesis protein)	4	0,798	0,030	**0,652**	0,013
ARTHROv5_60133|ID:18398638|chlB|	A0A9P1P131	ChlB	Light-independent protochlorophyllide reductase subunit B (LI-POR subunit B) (DPOR subunit B)	2	1,030	NS	**0,497**	0,037
ARTHROv5_12000|ID:18395419|atpC|	A0A9P1NYV2	AtpC	ATP synthase epsilon chain	2	0,866	NS	**0,642**	0,035
ARTHROv5_12001|ID:18395420|atpD|	A0A9P1NY47	AtpD	ATP synthase F1 complex subunit beta	19	0,827	NS	**0,570**	0,002
ARTHROv5_60533|ID:18399038|atpG2|	A0A9P1KLH7	AtpG2	ATP synthase B' chain (Subunit II)	5	0,891	NS	**0,648**	0,001
ARTHROv5_60535|ID:18399040|atpH|	A0A9P1P1N5	AtpH	ATP synthase delta chain; ATP synthase F1, delta subunit	7	0,804	NS	**0,609**	0,001
ARTHROv5_60537|ID:18399042|atpG1|	A0A9P1P0X3	AtpG1	F1 sector of membrane-bound ATP synthase, gamma subunit	4	0,863	NS	**0,622**	0,005
Nitrogen metabolism								
ARTHROv5_11880|ID:18395299|cynS|	A0A9P1KDV9	CynS	cyanase	2	1,565	NS	**2,847**	0,007
ARTHROv5_12133|ID:18395552|glnA|	A0A9P1NXZ0	GlnA	glutamine synthetase	11	1,483	NS	**1,989**	0,012
ARTHROv5_50271|ID:18398407|glnB|	A0A9P1P0D2	GlnB	Signal transduction protein P-II, Nitrogen metabolism regulatory protein	4	1,271	NS	**1,536**	0,004
Other								
ARTHROv5_60290|ID:18398795|	A0A9P1P1H0		conserved protein - TPM domain-containing protein	6	0,813	0,006	**0,656**	0,002
ARTHROv5_30321|ID:18396150|lytE|	A0A9P1KF76	LytE	Endopeptidase, cell wall lytic activity	3	0,729	0,049	**0,635**	0,027
ARTHROv5_11505|ID:18394924|clpP4|	A0A9P1KDE1	ClpP4	proteolytic subunit of ClpA-ClpP and ClpX-ClpP ATP-dependent serine proteases	4	**1,503**	0,041	1,426	NS
ARTHROv5_60998|ID:18399503|	A0A9P1KKY3		conserved protein (secreted) - alpha/beta hydrolase	6	1,557	NS	**2,307**	0,033
ARTHROv5_61085|ID:18399590|	A0A9P1P1E6		outer envelope membrane protein	4	ND	ND	**1,539**	0,032
ARTHROv5_11955|ID:18395374|	A0A9P1KD39		conserved protein - *R3H domain-containing nucleic acid-binding protein*	2	**1,644**	0,031	**1,488**	0,033
ARTHROv5_60179|ID:18398684|	A0A9P1KJQ0		putative SAM-dependent methyltransferase - *class I SAM-dependent methyltransferase*	2	1,027	NS	**1,458**	0,006
ARTHROv5_60282|ID:18398787|rpaB|	A0A9P1KKN3	RpaB	Redox-Responsive Transcription Factor - response regulator transcription factor	2	0.977	NS	**1.602**	0.002

578

The protein profile for the photosynthetic metabolism showed a modification regarding the light flux intensity increment in cycle 3 and 4 (Figure 7). Within cycle 3, two photosynthetic proteins with different expression levels compared to the control group (cycle 1) were observed. These proteins, belonging to the phycobilisome, demonstrated a lower expression with increasing light intensity (Table 2). In addition, two proteins in cycle 3 showed an expression close to the commonly accepted low threshold (Table 2), one belonging to the photosystem I and one to pigment synthesis pathway. Within cycle 4, 19 proteins demonstrated a lower expression. Amongst the impacted proteins, five belonged to the phycobilisome light harvesting antenna, four to photosystem II, three to photosystem I, and five to the ATP synthase (Table 2). As expected, these results show a reduction of the photosynthetic metabolism with increasing light, through the reduction of the phycobilisome (cycle 3 and 4), the photosystem II (cycle 4), photosystem I (cycle 4), and ATP synthase (cycle 4) proteins.

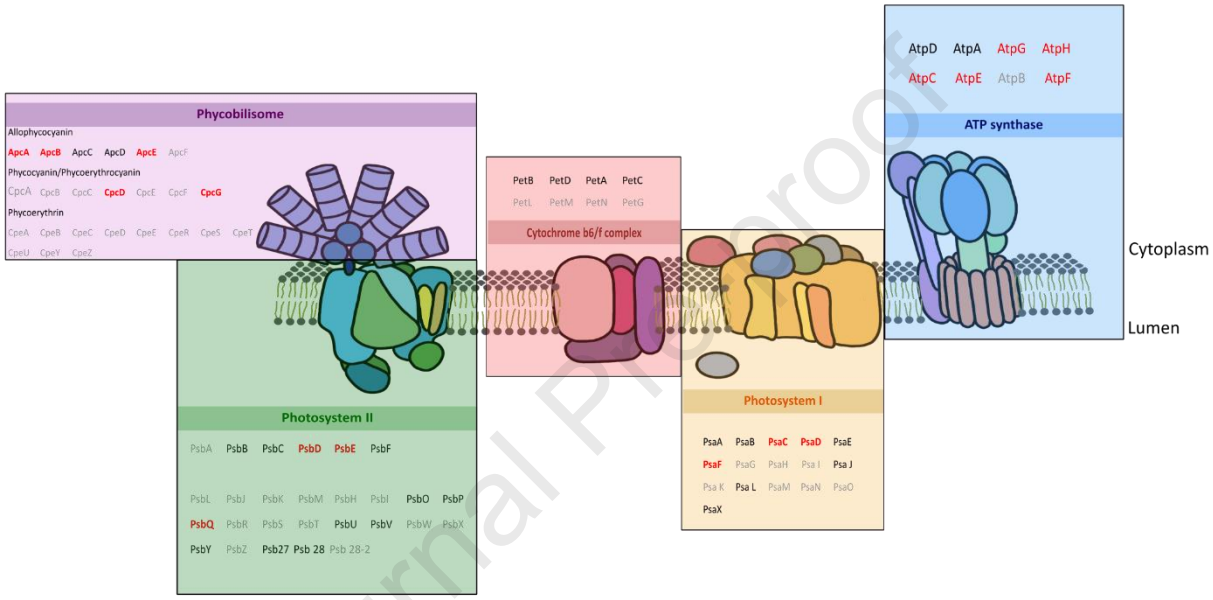

Figure 7. Schematic representation of the photosynthetic apparatus displaying proteins with a lower expression distribution in cycle 4 compared to cycle 1. (Red = fold change ≤ 0.66, Orange = fold change ≤ 0.8, grey = not detected in this analysis, black = detected in this analysis.

Another interesting finding was the higher expression of the redox response regulator RpaB protein in cycle 4. In *Synechocystis*, this protein was found to be an important transcriptional regulator for the expression of the phycobilisome proteins, photosystem II and I proteins, proteins of the electron transport chain, and many more (Riediger et al. (2019). In this study, the photosynthesis related proteins PsaD, PsaF, CpcG and ApcE were all found to be downregulated in C4 *vs* C1. According to (Riediger et al. 2019), a higher abundance of RpaB should induce the production of these proteins. Additionally, several of the proteins that should be regulated by RpaB were detected and identified but not differentially expressed. Thus, a conclusion on whether the RpaB protein acts as a regulator of photosynthesis in the present study cannot be drawn. In addition, the proteomic results demonstrated a higher expression of proteins associated with nitrogen assimilation, with increasing light. Three proteins, including the cyanase (CynS), the glutamine synthetase (GlnA) and the protein P-II (GlnB), were in higher abundance detected in cycle 4 compared to cycle 1 (Table 2). Moreover, a general tendency is observed amongst all cycles for these three proteins when disregarding the *p-value* significance. These results suggest an increase in both nitrogen assimilation and storage mobilisation with increasing light intensity.

Lastly, structural proteins as well as domain-containing proteins (classed as “structural” and “others” in the repository MSV000094881) showed an interesting modification in the cycles with higher light

intensity when compared to the cycle 1 as control. A great majority of these proteins has demonstrated a higher expression. However, the function of these proteins within the cell is not yet known.

3.3 SVT Lipidomic characterisation

The lipidomic analysis was conducted to characterise the overall lipid population in *L. indica* cells cultivated within the bioreactors. As for proteomic analysis, the samples of GM02, which were not axenic, were not considered in this analysis. The analysis was focused on the comparison of cycle 3 and 4 *vs* cycle 1, to assess the impact of higher light intensity on the lipid composition. The analysis has revealed the presence of lipids of all six main lipid classes following the classification proposed by Fahy et al. (2011): fatty acyls [FA], glycerolipids [GL], glycerophospholipids [GP], sphingolipids [SP], sterol lipids [ST] and prenol lipids [PR] (Figure 8). There was no difference in relative abundance of each lipid class, detected for any of the classes, in negative mode (Fatty Acyls (*p-value* = 0.66), Glycerolipids (*p-value* = 0.86), Glycerophospholipids (*p-value* = 0.72), and Sphingolipid (*p-value* = 0.73), Sterol (*p-value* = 0.87)) or positive mode (Fatty Acyls (*p-value* = 0.95), Glycerolipids (*p-value* = 0.52), Glycerophospholipids (*p-value* = 0.38), and Sphingolipid (*p-value* = 0.49), Sterol (*p-value* = 0.16), Prenol (*p-value* = 0.85)).

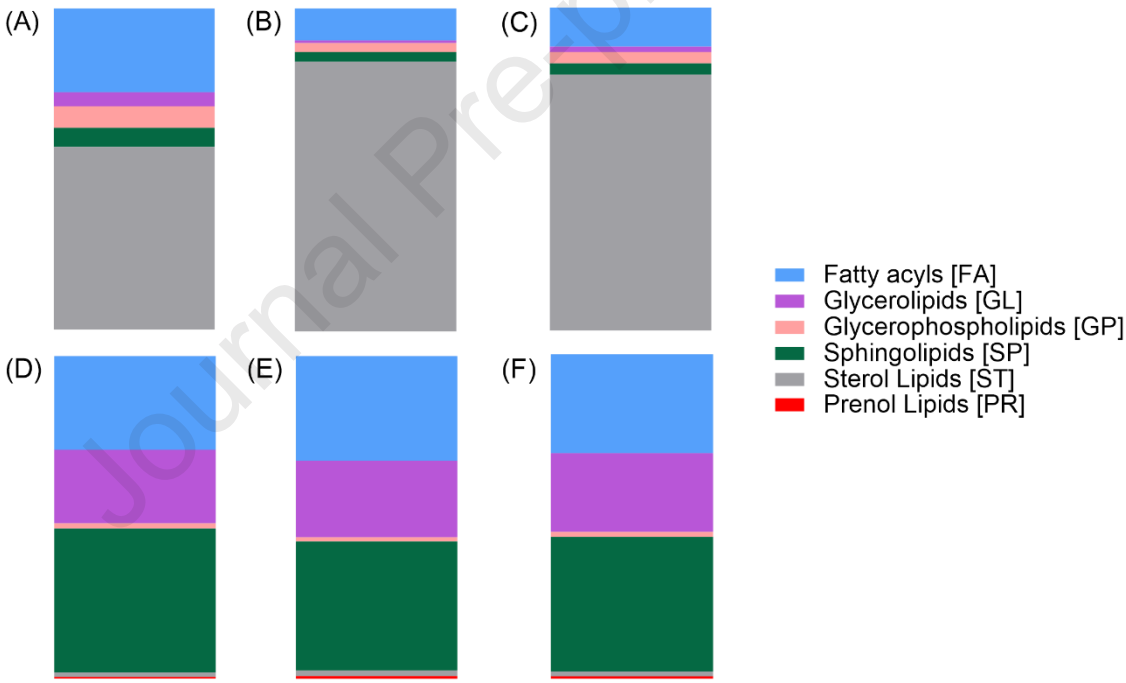

Figure 8. Lipid composition of *L. indica* PCC8005 P3 based on the main classes of lipids defined by Fahy et al. (2011). (A) and (D) Cycle 1, (B) - (E) Cycle 3, (C) - (F) Cycle 4. (A) to (C) = Negative mode, (D) to (F) = Positive mode.

4. Discussion

The data collected from this study have been crucial for refining the hardware and ensuring the scientific objectives of the mission are met. Technical issues related to PBRs contamination and leakage have been addressed through the run of the SVT/δ-SVT experiments. Nevertheless, the purpose of this study was not only to address technical challenges but to lay the groundwork for the next phase of experiments, which will include both in-space and on Earth-based setups.

4.1 Oxygen and biomass productivities

In the previous space flight of ArtB, 4 PBRs were run on board the ISS in batch mode, and 4 PBRs were run on ground, in parallel. Each of these 8 reactors was planned to conduct 4 batches, meaning that in total, 32 different batches could be compared on r_{O2}, r_X and $Y_{O2/X}$, as well as OD. Beforehand, the model developed at the University of Clermont-Auvergne (UCA) was used to predict the bioprocess (Poughon et al. 2021; Poughon et al. 2020). In ArtB, 3 of the 32 batches reached the expected r_{O2} of 0.33 mmol L^{-1} h^{-1}, the other batches showed lower than expected r_{O2} values (Poughon et al. 2020). The reasons were presumably technical issues like gas and liquid leakages, stirring problems and pressure sensor malfunctions. The results from the previous flight experiment provoked minor hardware adaptions which were performed in parallel to the adaptions to switch from a batch regime (ArtB) to a semi-continuous regime (ArtC). These adaptations included the relocation of the pump to upfront of the CC, a higher stirrer speed (1000 rpm instead of 800 rpm) and the use of different feed reservoirs. Additionally, the kinetic model of ArtB was adapted to fit the new regime of ArtC (e.g. inclusion of dilution rate). The development of a biological life support system is a flowing process, and each experiment helps to improve the overall functionality. Two of the main goals of the experiments presented in this study are to provide further hands-on knowledge and pathing the way towards a successful ArtC space flight experiment, because SVT and δ-SVT form the bridge between ArtB and ArtC. In the batch phase of SVT r_{O2} values between 0.10 ± 0.03 (GM04) and 0.25 ± 0.01 mmol L^{-1} h^{-1} (GM02) were found and in δ-SVT, the values were between 0.13 ± 0.00 (GM01) and 0.29 ± 0.00 (GM02) mmol L^{-1} h^{-1}, which was lower than expected. In addition, it has to be taken into account that the light intensity was higher than during ArtB (ArtB: 35 µmol m^{-2} s^{-1}, ArtC batch: 45 µmol m^{-2} s^{-1}).

The SVT and δ-SVT experiments showed a successful storage (only SVT), revival and batch propagation. Also, oxygen and biomass production over the course of 9 and 5 weeks in semi-continuous mode were achieved. ARTHROSPIRA-B and –C are proof-of-principle experiments, aiming to investigate the photosynthetic bioprocess of *L. indica* under space conditions with a low light flux intensity (35-80 µmol photons m^{-2} s^{-1}) and warm temperature (33°C) set-up. Thus, SVT and δ-SVT are also not aiming at producing oxygen and biomass to supply a space crew, but to proof reliability of the hard- and software and an active photosynthetic bioprocess within the photobioreactors (PBRs). The O_2 production rates (average: 0.32 mmol L^{-1} h^{-1}) achieved with the space hardware indicate that a liquid volume of ~3400L would be needed to support one space traveller, based on the assumption that one human needs ~0.82 kg O_2 d^{-1} (Anderson, Ewert, and Keener 2018). Therefore, a scale up of the system is one of the necessary steps that need to be taken during the further development of the MELiSSA loop. In a final life support system, much higher light fluxes (probably > 1000 µmol photons m^{-2} s^{-1}) and optimised gas transfer systems will be used to reach high oxygen and biomass production rates (aiming for ~200L reactors per space traveller). First steps towards this scale-up are already investigated. It could be shown by Alemany et al. (2019) that their 83 L external-loop gas lift PBR is able to produce 5-10% of the O_2 needed by one human. In these first experiments, they provided three Wistar rats with sufficient O_2 by a dynamic adaptation of light intensity depending on the O_2 need of the rats, an important first step towards a successful scale-up.

During SVT and δ-SVT, an increase in OD, r_X, r_{O2} was expected with increasing light flux intensity. The increasing light conditions are normally inducing higher growth rates and therefore higher OD values and oxygen production, when the photon flux is the limiting parameter (Fahrion, Dussap, and Leys 2023; Cornet and Dussap 2009). The results showed that most measured parameters stagnated between the different light intensities and for r_{O2} and $Y_{O2/X}$ of SVT, a zig-zag pattern was found. Table 1 shows additionally, that the r_{O2} and $Y_{O2/X}$ values are lower than predicted by the model. The stagnation of OD, r_X, r_{O2} can be explained by inhibiting oxygen levels in the liquid phase caused by an insufficient gas transfer. This causes a growth kinetics which is controlled by the gas transfer of O_2 from the liquid phase to the gas compartment by diffusion through the membrane instead of by the light intensity. Several observations lead to this hypothesis of oxygen inhibition and oxygen bubble formation inside the liquid compartment. Firstly, Figure 5 showed a deflation of the CC bags after SVT, proofing a loss of liquid volume over time and indicating a distorted ratio between gas and liquid

pressure. One of the reasons for this loss of liquid are the reservoirs exchanges after each cycle which caused an underpressure at the waste side of the reactors, pulling liquid from the CC. A liquid pressure below the gas pressure inhibits a sufficient O_2 release, which manifests as low r_{O2} values which can even decrease over time (Fig. 2). Additionally, the insufficient gas release can cause bubbles in the CC (Fig. 5, SVT and δ-SVT). The loss of liquid volume in combination with the bubble formation causes an oxygen oversaturation in the liquid phase, inhibiting the cells due to an emerging competition between CO_2 and O_2 at RuBisCo level (Iñiguez et al. 2020). Bubble formation also causes an underestimation of the oxygen production because all oxygen which is trapped in bubbles results in a higher gas volume and a lower liquid volume. Consequently, the produced oxygen per unit of total CC (liquid) volume is very significantly underestimated considering the total volume of gas phase is higher than expected (V_G = 22.37 mL) and the total volume of liquid is lower than the theoretical liquid volume (V_L = 59.25 mL). It also must be considered that the OD measurements do indicate a true biomass concentration. The underestimated r_{O2} values, also lead to an underestimation of the oxygen yield per gram biomass ($Y_{O2/X}$) that is lower than would be expected based on the stoichiometric equation. Additionally, an off-gassing of O_2 via the liquid tubing walls may be considered, but due to the low O_2 permeability of BPT tubing material, it can be assumed that a loss of gas via the tubing is small to negligible.

Since the loss of liquid volume during SVT caused difficulties to obtain reliable r_{O2} and $Y_{O2/X}$ values, there were some propositions for improvement put into place to investigate the root causes and improvements for δ-SVT and the upcoming space flight experiment ArtC. Small software adaptations were made to avoid timeline errors and a different reservoir handling procedure was put into place to circumvent development of an underpressure at the waste site. The latter approach was supported by manual filling commands before sampling and reservoir exchange, to additionally maintain the liquid pressure (5 min filling without outflow at 3 mL min^{-1} pump speed). To improve the precision of the OD values and to circumvent high standard deviations, we performed new calibrations before the next experiment (δ-SVT) started. It was shown that the electronics transmitting the OMU signals to the computers is heat sensitive, and the problem improved after the electronics were removed from the incubator. Figures 5 shows that the improvements put into place for δ-SVT resulted in CCs which are not deflated anymore at the end of the experiment. Only a few bubbles can be seen in GM01. It must be mentioned that at the start of cycle 1, GM01 had to be opened and the CC was found to be deflated to approximately 50% of its original volume, due to a problem with one of the reservoirs. This problem could fortunately be solved by the addition of fresh Zarrouk medium. Nevertheless, after cycle 1, small gas bubbles were detected in the CC of GM01, similar to the end point (Figure 5). Unfortunately, the CCs of the reactors cannot be checked for deflations or bubbles during an active cycle, therefore it cannot be excluded that a deflation or bubbles occurred in one of the CCs during δ-SVT. The r_{O2} and $Y_{O2/X}$ values of δ-SVT indicate that the gas transfer from the culture chamber to the gas compartment is still not optimal and the cells are experiencing oxygen inhibition, similar to SVT. Additionally, the photographs of SVT and δ-SVT showed that the assumption of the model of a homogeneous liquid phase cannot be fully met in the practical set-up, also causing possible discrepancies between modelled and practical values.

Due to a software error, there was a period at the end of cycle 3 of SVT where the light and pump settings of all 4 reactors were incorrect. During this time, the pump ran at an increased speed (~2.2 ml h^{-1} for ~24 h), causing a strong dilution of the cultures which was also measured as additional weight in the waste side of the reservoirs (~39 mL more flow through than expected). The light flux intensity was decreased to approximately ~25 µmol photons m^{-2} s^{-1} during this period. *L. indica* switches from dark respiration to photosynthetic growth at approximately 5 W m^{-2} (~23 µmol photons m^{-2} s^{-1}) (Cogne, Gros, and Dussap 2003; Cornet et al. 1992), meaning that the low light flux intensity during the incorrect settings induced a very slow photosynthetic growth rate. This probably caused the drop in r_{O2} and $Y_{O2/X}$ between cycle 2 and 3 (55 and 70 µmol photons m^{-2} s^{-1}, Fig. 2). The increase of these parameters in cycle 4 (80 µmol photons m^{-2} s^{-1}) supports the hypothesis that the cultures recovered after the incident.

In δ-SVT, one reactor was used for 3 days to test a 50 mbar instead of 150 mbar threshold. It was observed that the lower threshold is feasible for the soft- and hardware. In a next experiment, the lower threshold will be used during the entire experiment run, because this could help to ensure that the gas pressure stays below the liquid pressure, and this change was shown to be easy to implement. This adaptation is currently planned for the upcoming experiment sequence test (EST).

The biomass production rates r_X were in the expected range of 0.010 – 0.016 g L^{-1} h^{-1}. Cornet and Dussap (2009) tested the biomass productivity of *L. indica* PCC8005 in eight different photobioreactors, assessing the influence of light flux intensity, geometry, and operation modus to build a prediction formula for the maximum volumetric productivities. In continuous regimes, they found r_X values between 8.0 ± 0.7 * 10^{-3} kg m^{-3} h^{-1} and 19.0 ± 0.2 * 10^{-3} kg m^{-3} h^{-1} (0.008 ± 0.007 g L^{-1} h^{-1} and 0.019 ± 0.002 g L^{-1} h^{-1}). The biomass production rates in SVT and δ-SVT were found to be between 0.008 ± 0.000 and 0.021 ± 0.002 g L^{-1} h^{-1} and therefore in the same range.

The QY measurements were in the expected range in both SVT and δ-SVT, as the values for healthy cyanobacteria usually lie between 0.3 and 0.6 (Gao, Yu, and Brown 2007; Masojídek, Vonshak, and Torzillo 2010; Allahverdiyeva et al. 2013; Schuurmans et al. 2015). For batch cultures of *L. indica* PCC8005 P3 the QY range was previously shown to be 0.3 and 0.5 (Fahrion, Dussap, and Leys 2023), supporting the hypothesis that a successful photosynthetic bioprocess could be maintained during SVT and δ-SVT. In both experiments discussed here, axenicity could be proven for 3 out of 4 reactors, and it was shown that the non-axenic reactors had the contamination in the hardware before the start of the experiments as inocula were contaminant free. This is indicating that optimisation and validation of sterilisation procedures, reaching all corners of the complex space hardware set-up, as well as post sterilisation sterility checks are of utmost importance. An additional sterilization step could circumvent this problem.

All online parameters assessed during these experiments showed a high variability in between the different reactors. Thus, the data sets of the reactors should not only be combined to receive an overview of the production rates, but also be viewed independently to assess the results.

In general, the results of the online data of SVT and δ-SVT helped to uncover problems and provided knowledge on possible solution approaches. These data sets lead to an approval for continuation of ArtC for space flight by ESA.

4.2 Protein and lipid composition of produced Biomass

The proteomic results revealed the adaptation of *L. indica* PCC 8005 metabolism within ARTHROSPIRA-C Ground Model Demonstrator system to varying light flux intensity, between 45 and 80 µmol photons m^{-2} s^{-1}. Among others, the photosynthesis and the nitrogen assimilation pathways were significantly impacted.

4.2.1 Effect of light flux increase on the photosynthetic pathway

The adaptation to fluctuating light levels is crucial for photosynthetic organisms' survival, as improper regulation of photosynthesis and its components can lead to cellular damage due to reactive oxygen species (Pandhal, Wright, and Biggs 2007). As expected, the proteomic analysis revealed a significant reduction in the photosynthetic metabolism when exposed to an increasing light flux intensity. Indeed, in cycle 3 and 4, several key photosynthetic protein complexes presented a lower expression compared to the control cycle (cycle 1). Proteins including components of the phycobilisome light harvesting antenna, the photosystem II, the photosystem I, the cytochrome electron transport chain, and the ATP synthase, all exhibited a lower expression (Figure 7). Similar results have already been observed in analyses involving *L. indica* where it has been shown that exposing cells to increasing varying light intensities can cause a significant decrease in the efficiency of solar energy conversion during

photosynthesis (Vonshak et al. 1996; Jensen and Knutsen 1993) and is consistent with observations made at the transcriptomic level within *Synechococcus sp*. PCC 7002 strain (Xiong et al. 2015). This decrease in the abundance of photosynthetic proteins suggests an adaptation of the cells towards a lower photon absorption and lower photosynthetic activity during the experiments in response to the increase in light flux intensity imposed in the consecutive process cycles (Vonshak et al. 2014; Vonshak et al. 1996). These findings align with the results showing a lower OD measurement for chlorophyl and phycocyanin (Figure 3) and a lower quantum yield (Figure 4) is observed with a higher light intensity. Overall, the decrease in photosynthetic proteins aligns with the light availability in the experimental cycles, suggesting an adaptive response of the organism to optimise its energy utilisation under varying light conditions.

4.2.3 Effect of light flux increase on nitrogen assimilation pathway

Nitrogen is an essential and available through various forms: nitrates, ammonia, or organic nitrogen (Barrios-González 2018; Shabb, Muhonen, and Mehus 2017; Flores et al. 2005; Flores and Herrero 1994). Our analysis revealed an increase in the expression of proteins related to nitrogen assimilation metabolism when exposed to higher light flux (in cycle 3 and 4) in comparison to the cycle with lower light flux (cycle 1). The elevated levels of proteins involved in nitrogen assimilation indicate an enhanced cellular demand for nitrogen-related processes. Inorganic nitrogen in the form of ammonium is assimilated into glutamine via the glutamine synthetase cycle. The protein P-II involved in the regulation of glutamine synthase activity (Bolay et al. 2018; de Zamaroczy, Delorme, and Elmerich 1990), exhibited a higher expression in cycle 4. Additionally, it has been observed in plants that glutamine synthetase activity plays a role in control of photosynthetic responses to high light (Brestic et al. 2014). Cyanase, observed with a higher expression in cycle 4, is known for its role in ammonium production through the cyanate catalysis. This cyanase enzyme is been reported to be also present and functional in the *Synechococcus* sp. strain PCC6301, for which cyanate has been shown to be a potential nitrogen source (Kamennaya and Post 2011; Kamennaya, Chernihovsky, and Post 2008).

In cyanobacteria, photosynthesis relies on large membrane-embedded protein complexes, including photosystems (PSII and PSI), cytochromes b6, and ATPase, which are specialised in converting sunlight into chemical energy (Battchikova, Angeleri, and Aro 2015). The reduction in activity of the photosynthetic metabolism, associated with the increased nitrogen metabolism pathway reveal a metabolic adaptation by the culture of *Limnospira indica* under higher luminous intensity conditions.

4.2.4 Lipidomic characterisation

Lipids play a role in various biological processes, including membrane structure, energy storage, and cellular signalling (Lomba-Riego, Calvino-Sanles, and Brea 2022; Santos and Preta 2018). The composition of fatty acids directly depends on the organisms growth conditions, reflecting cellular responses and adaptations to the surrounding environment (Da Costa et al. 2016).

The lipidomic analysis (Figure 8) reveals the presence of lipids from all six main lipid classes, which were also identified in *Spirulina platensis* by Ramadan and Selim Asker (2008). The relative abundance of the main lipid categories identified during the SVT experiment remained stable across the four cycles, with no significant variations observed. This rather constant lipid composition in all light flux intensity conditions suggests a stable lipidomic profile regardless of the increasing light flux. It is important to note that significant environmental stress, such as salt stress, or light intensity has been

shown to induce an increase in lipid biosynthesis in *L. indica* as well as an increasing proportion of fatty acid (Tedesco and Duerr 1989). The stability of lipid composition in our analysis demonstrates the absence of stress response to increased light flux at the lipidomic level. The constant abundance of all lipid classes across the cycles suggests that the light intensity used does not affect the lipids composition of *L. indica* PCC 8005. The uniformity in lipids relative abundance implies a well-regulated biosynthesis and turnover of lipids within the cells, ensuring the maintenance of essential lipid functions and structural integrity.

These results suggest that the nutritive value related to the lipids remained also constant within the range of light intensities used for the SVT demonstration. Glycolipids from cyanobacteria, including lipids classes such as sphingolipids, glycolipids and glycerophospholipids, are an important source of n-3 fatty acids with beneficial health implications to humans (Da Costa et al. 2016). Additionally, some glycolipids extracted from microalgae and cyanobacteria possess various biological activities such as antifungal, antiviral and antitumoral properties (Plouguerné et al. 2014; Plouguerné et al. 2013; Naumann et al. 2007; Morimoto et al. 1995). Specifically, some fatty acids from *L. indica*, such as the stearic acid, a fatty acid also present in our analysis, has shown a promising impact as an immune system enhancer (Huh et al. 2022). Collectively, these results demonstrate the major interest to monitor the lipid composition in future life support systems.

5. Conclusion

In conclusion, the SVT and δ-SVT experiments have demonstrated the successful storage, revival, batch propagation as well as production of oxygen and biomass over extended durations (9 and 5 weeks), providing essential insights into the reliability of hardware and the active photosynthetic bioprocess within the space hardware. The axenicity verification and the identification of non-axenic reactors indicate the importance of additional sterilization steps to prevent contamination. While the experiments were not designed to produce sufficient oxygen and biomass for space crew supply, the O_2 production rates achieved offer insights into the scalability of the system for future space missions. These findings are an essential part of the development path towards biological life support systems in space.

The SVT experiment revealed challenges and areas for improvement, which were then addressed in the δ-SVT experiment and further improved for the upcoming space flight. The decrease in liquid volume influenced O_2 production rates and lead to the formation of bubbles within the culture chambers which resulted in oxygen limited growth kinetics. Software and handling procedures were adjusted to mitigate these issues and improve the precision of optical density measurements. These adaptations, as seen in δ-SVT, improved the results but did not fully resolve the problems, highlighting the importance of continuous improvement in experimental design. Biomass production rates were consistent with the modelled results. Additionally, quantum yield measurements fell within the expected range, suggesting the maintenance of a successful photosynthetic bioprocess during SVT and δ-SVT. Therefore, the data of the SVT/δ-SVT experiments reported in this manuscript are valuable not only as part of the of the space flight preparations but also in terms of biological response. Indeed, *Limnospira indica* is capable to grow over two months in a batch as well as continuous regime inside these reactors. Lastly, these results highlight that the gas transfer, in addition to the light transfer, is an important parameter to consider in the hardware design of such systems.

The proteomics analysis revealed an impact of varying light flux intensity on *L. indica* PCC 8005 metabolism. The photosynthetic pathway experienced a significant reduction under higher light

intensities, suggesting an adaptive response to optimise energy utilisation. Concurrently, an increased representation of nitrogen assimilation-related proteins indicated an enhanced need for nitrogen assimilation under the altered conditions. While these results present an adaptation to the current environment, these results do not exhibit a strong stress response as it is confirmed by the lipidomic analysis. Indeed, the lipidomic analysis showed that the lipid composition of *L. indica* remained consistent across all light flux intensities, indicating stable lipidomic profiles unaffected by the varying light intensity. These findings are valuable for understanding the nutritive value and potential applications of *L. indica* in future life support systems.

Overall, the SVT and δ-SVT experiments have provided crucial insights into the operation of life support systems for space missions and have identified areas for improvement and paved the way for the continuation of ArtC for space flight by ESA. ESA's approval to move forward attests to the robustness of the space hardware and the value of the data collected. The comparative experiments in space and on Earth will allow us to validate our conclusions and adjust for any space-specific response. This multi-phase approach, common in space mission research, ensures that both the hardware and scientific experiments and outcomes are well-prepared for the upcoming mission's success. These findings contribute to the ongoing development of bioreactors for sustainable life support in the challenging environment of space, marking significant progress toward enabling long-duration manned missions.

6. Acknowledgements

This article has been made possible through the authors involvement in the MELiSSA project, ESA's life support system program (https://www.esa.int/Enabling_Support/Space_Engineering_Technology/Melissa) and through the ARTEMiSS project (supported by ESA/PRODEX and BELSPO) providing the PhD grants of Jana Fahrion and Cécile Renaud. The Bioprofiling platform used for proteomic and lipid analysis was supported by the European Regional Development Fund and the Walloon Region, Belgium.

7. Disclosure statement

No potential conflict of interest was reported by the author(s).

8. Author contributions

JF and CR contributed equally to the data analysis as well as the writing of the first manuscript draft. IC, WH and JF conducted the experiment runs in the laboratory. CR performed the experimental work of proteomics and lipidomics analysis. JF analysed the online data received from the reactors. CGD helped with the analysis and interpretation of the online data. FM, SG, RW and GBV helped with the data analysis and interpretation of proteomics and lipidomics data. All authors contributed to reviewing, data interpretation and editing. NL was responsible for study and experiment conceptualisation, the funding acquisition for this research, and the project management with the space agency, the payload developer, and the scientific partners.

9. References

Alemany, Laura, Enrique Peiro, Carolina Arnau, David Garcia, Laurent Poughon, Jean-François Cornet, Claude-Gilles Dussap, Olivier Gerbi, Brigitte Lamaze, Christophe Lasseur, and Francesc Godia. 2019. 'Continuous controlled long-term operation and modeling of a closed loop connecting an air-lift photobioreactor and an animal compartment for the development of a life support system', *Biochemical Engineering Journal*, 151.

Allahverdiyeva, Yagut, Henna Mustila, Maria Ermakova, Luca Bersanini, Pierre Richaud, Ghada Ajlani, Natalia Battchikova, Laurent Cournac, and Eva-Mari Aro. 2013. 'Flavodiiron proteins Flv1 and Flv3 enable cyanobacterial growth and photosynthesis under fluctuating light', *Proceedings of the National Academy of Sciences*, 110: 4111-16.

Anderson, Molly S.;, Michael K.; Ewert, and John F. Keener. 2018. 'Life Support Baseline Values and Assumptions Document'.

Barrios-González, Javier. 2018. 'Secondary metabolites production: physiological advantages in solid-state fermentation', *Current developments in biotechnology and bioengineering*: 257-83.

Battchikova, Natalia, Martina Angeleri, and Eva-Mari Aro. 2015. 'Proteomic approaches in research of cyanobacterial photosynthesis', *Photosynthesis research*, 126: 47-70.

Bolay, Paul, M Isabel Muro-Pastor, Francisco J Florencio, and Stephan Klähn. 2018. 'The distinctive regulation of cyanobacterial glutamine synthetase', *Life*, 8: 52.

Brestic, Marian, Marek Zivcak, Katarina Olsovska, Hong-Bo Shao, Hazem M Kalaji, and Suleyman I Allakhverdiev. 2014. 'Reduced glutamine synthetase activity plays a role in control of photosynthetic responses to high light in barley leaves', *Plant Physiology and Biochemistry*, 81: 74-83.

Cogne, G, Ch Lasseur, J-F Cornet, C-G Dussap, and J-B Gros. 2001. 'Growth monitoring of a photosynthetic micro-organism (Spirulina platensis) by pressure measurement', *Biotechnology letters*, 23: 1309-14.

Cogne, G., J. F. Cornet, and J. B. Gros. 2005. 'Design, operation, and modeling of a membrane photobioreactor to study the growth of the Cyanobacterium Arthrospira platensis in space conditions', *Biotechnol Prog*, 21: 741-50.

Cogne, G., J. B. Gros, and C. G. Dussap. 2003. 'Identification of a metabolic network structure representative of Arthrospira (spirulina) platensis metabolism', *Biotechnol Bioeng*, 84: 667-76.

Cogne, G., B. Lehmann, C. G. Dussap, and J. B. Gros. 2003. 'Uptake of macrominerals and trace elements by the cyanobacterium Spirulina platensis (Arthrospira platensis PCC 8005) under photoautotrophic conditions: culture medium optimization', *Biotechnol Bioeng*, 81: 588-93.

Cornet, J-F, CG Dussap, and J-B Gros. 1998. 'Kinetics and energetics of photosynthetic micro-organisms in photobioreactors.' in, *Bioprocess and algae reactor technology, apoptosis* (Springer).

Cornet, Jean-François, and Claude-Gilles Dussap. 2009. 'A simple and reliable formula for assessment of maximum volumetric productivities in photobioreactors', *Biotechnology progress*, 25: 424-35.

Cornet, JF, CG Dussap, P Cluzel, and G Dubertret. 1992. 'A structured model for simulation of cultures of the cyanobacterium Spirulina platensis in photobioreactors: II. Identification of kinetic parameters under light and mineral limitations', *Biotechnology and bioengineering*, 40: 826-34.

Da Costa, Elisabete, Joana Silva, Sofia Hoffman Mendonça, Maria Helena Abreu, and Maria Rosário Domingues. 2016. 'Lipidomic approaches towards deciphering glycolipids from microalgae as a reservoir of bioactive lipids', *Marine Drugs*, 14: 101.

de Zamaroczy, Miklos, Frédéric Delorme, and Claudine Elmerich. 1990. 'Characterization of three different nitrogen-regulated promoter regions for the expression of glnB and glnA in Azospirillum brasilense', *Molecular and General Genetics MGG*, 224: 421-30.

Dou, Guiming, Hongcan Liu, Wei He, and Yuchao Ma. 2016. 'Bacillus lindianensis sp. nov., a novel alkaliphilic and moderately halotolerant bacterium isolated from saline and alkaline soils', *Antonie Van Leeuwenhoek*, 109: 149-58.

Fahrion, Jana, Claude Gilles Dussap, and Natalie Leys. 2023. 'Biological oxygen production in Space: Assessment of the right conditions in cyanobacterial batch cultures', *Frontiers in Astronomy and Space Sciences*, 10: 121.

Fahrion, Jana, Felice Mastroleo, Claude-Gilles Dussap, and Natalie Leys. 2021. 'Use of photobioreactors in regenerative life support systems for human space exploration', *Frontiers in Microbiology*, 12: 699525.

Fahy, Eoin, Dawn Cotter, Manish Sud, and Shankar Subramaniam. 2011. 'Lipid classification, structures and tools', *Biochimica et Biophysica Acta (BBA)-Molecular and Cell Biology of Lipids*, 1811: 637-47.

Farag, Mayada Ragab, Mahmoud Alagawany, Mohamed Ezzat Abd El-Hac, and Kuldeep Dhama. 2015. 'Nutritional and Healthical Aspects of Spirulina (Arthrospira) for Poultry, Animals and Human', *International Journal of Pharmacology*, 12: 36-51.

Flores, Enrique, José E Frías, Luis M Rubio, and Antonia Herrero. 2005. 'Photosynthetic nitrate assimilation in cyanobacteria', *Photosynthesis research*, 83: 117-33.

Flores, Enrique, and Antonia Herrero. 1994. 'Assimilatory nitrogen metabolism and its regulation.' in, *The molecular biology of cyanobacteria* (Springer).

Gao, Kunshan, Hongyan Yu, and Murray T Brown. 2007. 'Solar PAR and UV radiation affects the physiology and morphology of the cyanobacterium Anabaena sp. PCC 7120', *Journal of Photochemistry and Photobiology B: Biology*, 89: 117-24.

Hauslage, Jens, Sebastian M Strauch, Olaf Eßmann, Ferdinand WM Haag, Peter Richter, Julia Krüger, Julia Stoltze, Ina Becker, Adeel Nasir, and Gerhild Bornemann. 2018. 'Eu: CROPIS–"euglena gracilis: combined regenerative organic-food production in space"-a space experiment testing biological life support systems under lunar and martian gravity', *Microgravity Science and Technology*, 30: 933-42.

Hendrickx, L., H. De Wever, V. Hermans, F. Mastroleo, N. Morin, A. Wilmotte, P. Janssen, and M. Mergeay. 2006. 'Microbial ecology of the closed artificial ecosystem MELiSSA (Micro-Ecological Life Support System Alternative): reinventing and compartmentalizing the Earth's food and oxygen regeneration system for long-haul space exploration missions', *Res Microbiol*, 157: 77-86.

Huh, Jungmoo, Jin Zhang, Radka Hauerová, Joseph Lee, Saqlain Haider, Mei Wang, Tomáš Hauer, Ikhlas A Khan, Amar G Chittiboyina, and Nirmal D Pugh. 2022. 'Utility of fatty acid profile and in vitro immune cell activation for chemical and biological standardization of Arthrospira/Limnospira', *Scientific Reports*, 12: 15657.

Iñiguez, Concepción, Sebastià Capó-Bauçà, Ülo Niinemets, Heather Stoll, Pere Aguiló-Nicolau, and Jeroni Galmés. 2020. 'Evolutionary trends in RuBisCO kinetics and their co-evolution with CO2 concentrating mechanisms', *The Plant Journal*, 101: 897-918.

Jensen, Sigmund, and Gjert Knutsen. 1993. 'Influence of light and temperature on photoinhibition of photosynthesis in Spirulina platensis', *Journal of Applied Phycology*, 5: 495-504.

Junaedi, C., K. Hawley, D. Walsh, S. Roychoudhury, M. B. Abney, and J. L. Perry. 2011. "Compact and Lightweight Sabatier Reactor for Carbon Dioxide Reduction." In *41st International Conference on Environmental Systems*.

Kamennaya, Nina A, Mark Chernihovsky, and Anton F Post. 2008. 'The cyanate utilization capacity of marine unicellular Cyanobacteria', *Limnology and Oceanography*, 53: 2485-94.

Kamennaya, Nina A, and Anton F Post. 2011. 'Characterization of cyanate metabolism in marine Synechococcus and Prochlorococcus spp', *Applied and environmental microbiology*, 77: 291-301.

Lasseur, C., and M. Mergeay. 2021. 'Current and future ways to closed life support systems: virtual MELiSSA conference', *Ecological Engineering and Environment Protection*, 1: 75-85.

1009 Lasseur, Christophe. 2008. 'Melissa: The European project of a closed life support system', *37th*
1010 *COSPAR Scientific Assembly*, 37: 1706.
1011 Lomba-Riego, Lucia, Esther Calvino-Sanles, and Roberto J Brea. 2022. 'In situ synthesis of artificial
1012 lipids', *Current Opinion in Chemical Biology*, 71: 102210.
1013 MacLean, Brendan, Daniela M Tomazela, Nicholas Shulman, Matthew Chambers, Gregory L Finney,
1014 Barbara Frewen, Randall Kern, David L Tabb, Daniel C Liebler, and Michael J MacCoss. 2010.
1015 'Skyline: an open source document editor for creating and analyzing targeted proteomics
1016 experiments', *Bioinformatics*, 26: 966-68.
1017 Masojídek, Jiří, Avigad Vonshak, and Giuseppe Torzillo. 2010. 'Chlorophyll fluorescence applications
1018 in microalgal mass cultures.' in, *Chlorophyll a fluorescence in aquatic sciences: methods and*
1019 *applications* (Springer).
1020 Morimoto, Takashi, Akito Nagatsu, Nobutoshi Murakami, Jinsaku Sakakibara, Harukuni Tokuda,
1021 Hoyoku Nishino, and Akio Iwashima. 1995. 'Anti-tumour-promoting glyceroglycolipids from
1022 the green alga, Chlorella vulgaris', *Phytochemistry*, 40: 1433-37.
1023 Naumann, Ivonne, Kai H Darsow, Christian Walter, Harald A Lange, and Rainer Buchholz. 2007.
1024 'Identification of sulfoglycolipids from the alga Porphyridium purpureum by matrix-assisted
1025 laser desorption/ionisation quadrupole ion trap time-of-flight mass spectrometry', *Rapid*
1026 *Communications in Mass Spectrometry: An International Journal Devoted to the Rapid*
1027 *Dissemination of Up-to-the-Minute Research in Mass Spectrometry*, 21: 3185-92.
1028 Niederwieser, Tobias, Patrick Kociolek, and David Klaus. 2018. 'A review of algal research in space',
1029 *Acta Astronautica*, 146: 359-67.
1030 Nowicka-Krawczyk, P., R. Muhlsteinova, and T. Hauer. 2019. 'Detailed characterization of the
1031 Arthrospira type species separating commercially grown taxa into the new genus Limnospira
1032 (Cyanobacteria)', *Sci Rep*, 9: 694.
1033 Pandhal, Jagroop, Phillip C Wright, and Catherine A Biggs. 2007. 'A quantitative proteomic analysis of
1034 light adaptation in a globally significant marine cyanobacterium Prochlorococcus marinus
1035 MED4', *Journal of Proteome Research*, 6: 996-1005.
1036 Plouguerné, Erwan, Bernardo AP da Gama, Renato C Pereira, and Eliana Barreto-Bergter. 2014.
1037 'Glycolipids from seaweeds and their potential biotechnological applications', *Frontiers in*
1038 *cellular and infection microbiology*, 4: 174.
1039 Plouguerné, Erwan, Lauro M De Souza, Guilherme L Sassaki, Jéssica Figueiredo Cavalcanti, Maria
1040 Teresa Villela Romanos, Bernardo AP Da Gama, Renato Crespo Pereira, and Eliana Barreto-
1041 Bergter. 2013. 'Antiviral sulfoquinovosyldiacylglycerols (SQDGs) from the Brazilian brown
1042 seaweed Sargassum vulgare', *Marine Drugs*, 11: 4628-40.
1043 Poughon, L., C. Laroche, C. Creuly, C. G. Dussap, C. Paille, C. Lasseur, P. Monsieurs, W. Heylen, I.
1044 Coninx, F. Mastroleo, and N. Leys. 2020. 'Limnospira indica PCC8005 growth in
1045 photobioreactor: model and simulation of the ISS and ground experiments', *Life Sci Space Res*
1046 *(Amst)*, 25: 53-65.
1047 Poughon, Laurent, Catherine Creuly, Francesc Godia, Natalie Leys, and Claude-Gilles Dussap. 2021.
1048 'Photobioreactor Limnospira indica growth model: application from the MELiSSA plant pilot
1049 scale to ISS flight experiment', *Frontiers in Astronomy and Space Sciences*, 8: 700277.
1050 Ramadan, Mohamed Fawzy, and Mohsen Mohamed Selim Asker. 2008. 'Functional bioactive
1051 compounds and biological activities', *Czech J. Food Sci. Vol*, 26: 211-22.
1052 Riediger, Matthias, Taro Kadowaki, Ryuta Nagayama, Jens Georg, Yukako Hihara, and Wolfgang R
1053 Hess. 2019. 'Biocomputational analyses and experimental validation identify the regulon
1054 controlled by the redox-responsive transcription factor RpaB', *Iscience*, 15: 316-31.
1055 Santos, Ana L, and Giulio Preta. 2018. 'Lipids in the cell: organisation regulates function', *Cellular and*
1056 *Molecular Life Sciences*, 75: 1909-27.
1057 Schuurmans, R Milou, Pascal van Alphen, J Merijn Schuurmans, Hans CP Matthijs, and Klaas J
1058 Hellingwerf. 2015. 'Comparison of the photosynthetic yield of cyanobacteria and green algae:
1059 different methods give different answers', *PLoS One*, 10: e0139061.

1060 Shabb, JB, WW Muhonen, and AA Mehus. 2017. 'Quantitation of human metallothionein isoforms in
1061 cells, tissues, and cerebrospinal fluid by mass spectrometry.' in, *Methods in Enzymology*
1062 (Elsevier).
1063 Shitut, Shraddha, Meng-Jie Shen, Bart Claushuis, Rico JE Derks, Martin Giera, Daniel Rozen, Dennis
1064 Claessen, and Alexander Kros. 2022. 'Generating heterokaryotic cells via bacterial cell-cell
1065 fusion', *Microbiology Spectrum*, 10: e01693-22.
1066 Takada, Kevin, Steven Van Keuren, Luis Velasquez, Phillip Baker, and Stephen McDougle. 2019.
1067 "Advanced Oxygen Generation Assembly for Exploration Missions." In.: 49th International
1068 Conference on Environmental Systems.
1069 Tedesco, Mark A, and Eirik O Duerr. 1989. 'Light, temperature and nitrogen starvation effects on the
1070 total lipid and fatty acid content and composition of Spirulina platensis UTEX 1928', *Journal*
1071 *of Applied Phycology*, 1: 201-09.
1072 Tsugawa, Hiroshi, Tomas Cajka, Tobias Kind, Yan Ma, Brendan Higgins, Kazutaka Ikeda, Mitsuhiro
1073 Kanazawa, Jean VanderGheynst, Oliver Fiehn, and Masanori Arita. 2015. 'MS-DIAL: data-
1074 independent MS/MS deconvolution for comprehensive metabolome analysis', *Nature*
1075 *methods*, 12: 523-26.
1076 Tsugawa, Hiroshi, Kazutaka Ikeda, Mikiko Takahashi, Aya Satoh, Yoshifumi Mori, Haruki Uchino,
1077 Nobuyuki Okahashi, Yutaka Yamada, Ipputa Tada, and Paolo Bonini. 2020. 'A lipidome atlas in
1078 MS-DIAL 4', *Nature biotechnology*, 38: 1159-63.
1079 Vallenet, David, Laurent Labarre, Zoe Rouy, Valerie Barbe, Stephanie Bocs, Stephane Cruveiller,
1080 Aurelie Lajus, Geraldine Pascal, Claude Scarpelli, and Claudine Medigue. 2006. 'MaGe: a
1081 microbial genome annotation system supported by synteny results', *Nucleic acids research*,
1082 34: 53-65.
1083 Vonshak, Avigad, Lakkana Chanawongse, Boosya Bunnag, and Morakot Tanticharoen. 1996. 'Light
1084 acclimation and photoinhibition in three Spirulina platensis (cyanobacteria) isolates', *Journal*
1085 *of Applied Phycology*, 8: 35-40.
1086 Vonshak, Avigad, Supat Laorawat, Boosya Bunnag, and Morakot Tanticharoen. 2014. 'The effect of
1087 light availability on the photosynthetic activity and productivity of outdoor cultures of
1088 Arthrospira platensis (Spirulina)', *Journal of Applied Phycology*, 26: 1309-15.
1089 Wu, Qinghua, Lian Liu, Anca Miron, Blanka Klímová, Dan Wan, and Kamil Kuča. 2016. 'The
1090 antioxidant, immunomodulatory, and anti-inflammatory activities of Spirulina: an overview',
1091 *Archives of toxicology*, 90: 1817-40.
1092 Xiong, Qian, Jie Feng, Si-ting Li, Gui-ying Zhang, Zhi-xian Qiao, Zhuo Chen, Ying Wu, Yan Lin, Tao Li,
1093 and Feng Ge. 2015. 'Integrated Transcriptomic and Proteomic Analysis of the Global
1094 Response of Synechococcus to High Light Stress*[S]', *Molecular & Cellular Proteomics*, 14:
1095 1038-53.

1096

- Cyanobacterium *Limnospira indica* showed successful storage, revival, batch propagation and production of biomass and oxygen, when cultured in miniaturized photobioreactors over extended durations (9 and 5 weeks) in the pre-flight experiments with actual space flight hardware.
- The biomass production was in the expected range while the oxygen production was below the expected range.
- Proteomic analysis revealed an impact of varying light flux intensity on the photosynthetic carbon assimilation and nitrogen assimilation metabolic pathways.
- Lipidomic analysis showed that the lipid composition in the biomass remained consistent across all tested light flux intensities.

Declaration of interests

☒ The authors declare that they have no known competing financial interests or personal relationships that could have appeared to influence the work reported in this paper.

☐ The author is an Editorial Board Member/Editor-in-Chief/Associate Editor/Guest Editor for *[Journal name]* and was not involved in the editorial review or the decision to publish this article.

☐ The authors declare the following financial interests/personal relationships which may be considered as potential competing interests: